environments

MDPI

Review

Environmental Sustainability Based on Zirconium Dioxide Utilization in Non-Conventional Energy Applications

Ecaterina Matei [1], Anca-Andreea Șăulean [1,*], Mirela Petriceanu [2,3], Maria Râpă [1], Radu Robert Piticescu [3], Radu Ștefănoiu [1] and Cristian Predescu [1]

[1] Faculty of Material Science and Engineering, National University of Science and Technology POLITEHNICA Bucharest, 313 Splaiul Independentei, 060042 Bucharest, Romania
[2] Biotechnical Systems Engineering Doctoral School, National University of Science and Technology POLITEHNICA Bucharest, 313 Splaiul Independentei, 060042 Bucharest, Romania
[3] National Research&Development Institute for Non-Ferrous and Rare Metals—IMNR, 102 Biruinței Boulevard, 077145 Pantelimon, Romania
* Correspondence: andreea.turcanu90@yahoo.com

Abstract: The increasing demand for sustainable energy solutions has prompted a significant interest in non-conventional energy sources, leading to the development of innovative materials that can enhance energy conversion and storage efficiency. This review paper explores the pivotal role of zirconium dioxide (ZrO_2) in industrial applications related to non-conventional energy technologies, highlighting its contributions to the circular economy. We discuss various synthesis methods for ZrO_2, including top-down and bottom-up approaches, elucidating how these techniques influence the material's properties and applicability. Furthermore, we examine the unique characteristics of nano-ZrO_2 and its transformative potential in energy conversion and storage systems. By synthesizing current research findings, this review underscores the significance of ZrO_2 in promoting sustainable energy practices and its role in advancing the circular economy through material reuse and recycling strategies. The insights provided herein aim to inform future research directions and industrial applications, ultimately fostering a more sustainable energy landscape.

Keywords: zirconium dioxide; energy storage; energy conversion; top-down; bottom-up

check for updates

Citation: Matei, E.; Șăulean, A.-A.; Petriceanu, M.; Râpă, M.; Piticescu, R.R.; Ștefănoiu, R.; Predescu, C. Environmental Sustainability Based on Zirconium Dioxide Utilization in Non-Conventional Energy Applications. *Environments* **2024**, *11*, 265. https://doi.org/10.3390/environments11120265

Academic Editor: Joaquim Esteves Da Silva

Received: 15 October 2024
Revised: 18 November 2024
Accepted: 20 November 2024
Published: 22 November 2024

1. Introduction

One of the primary causes of global warming is the large-scale use of fossil fuels, which is why worldwide efforts are being made to introduce and use non-conventional energy sources, by which pollutants can be reduced and the maintenance of the average global temperature is possible. Energy storage technologies and conversion systems are necessary for its efficient use [1]. Non-conventional energy sources represent an alternative for the future, not only for a cleaner environment and economic sustainability but also for job creation. In this way, conventional sources such as coal, oil, fuel wood, thermal power plant, and nuclear energy could be replaced by non-conventional energy sources as solar, wind, tidal, geothermal energy, and biomass.

Today, a distinction is made between non-conventional energy sources in terms of green, clean, and renewable energy. Often, the terms "green" and "renewable energy" are used interchangeably, leading to confusion. While most green energies are renewable, not all renewables are considered green. Renewable energies refer to sustainable energies coming from naturally sources that renew themselves such as wind or solar energy. However, if carbon emissions are generated, renewable energy cannot be considered green energy. Clean energy is energy that does not produce greenhouse gas emissions, meaning some types of renewable energy are not clean. According to the world statistics data, hydropower is the largest modern renewable source, followed by wind and solar power, both of which are advancing fast as it can be seen in Figure 1 [2].

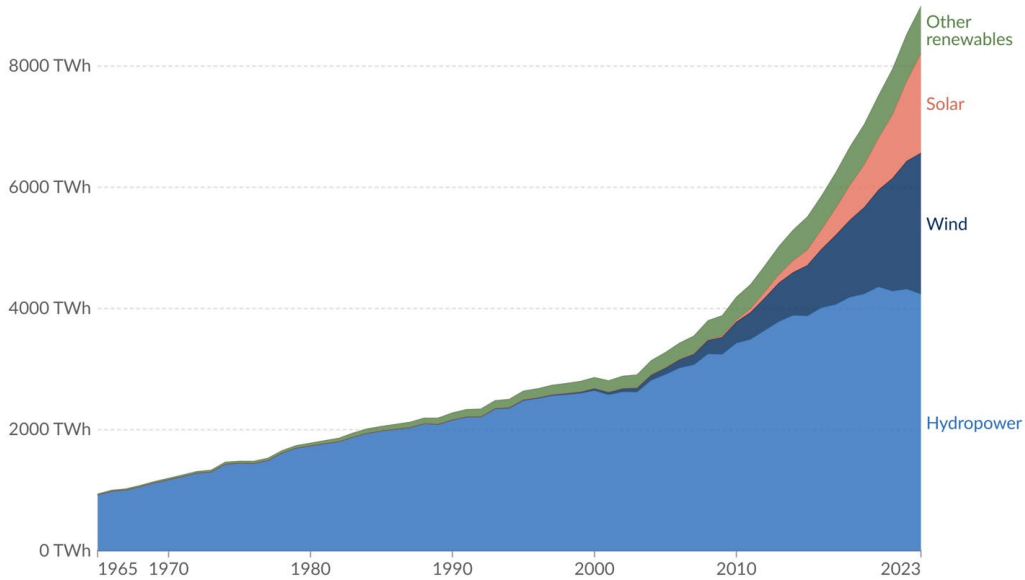

Figure 1. Renewable energy generation by hydropower, wind, solar, and other renewables (geothermal, biomass, waste, wave, and tidal) according to the World Statistics Data [2].

In many contexts, renewable and non-conventional energy sources are considered part of the same broader effort to develop cleaner and more sustainable energy systems. The distinction often depends on the specific technologies being discussed and their level of maturity and adoption in the energy market. To ensure the efficiency of these sources, durable energy materials are required for energy storage and conversion.

The future of non-conventional energy depends on the production and design of sustainable materials that are part of solar cells, combustion cells, batteries, supercapacitors, nanocomposites, etc. These materials correspond to the concept of clean energy, helping to reduce carbon and greenhouse gases, thus leading to a global economy free from CO_2. Generally, non-conventional energy sources obtained from the sun, wind, biomass, water, etc. contribute to global sustainable development [3]. Current lifestyle, consumption patterns, and industrial processes are decisive for global warming and require urgent changes in the production, storage, and supply of energy.

In this context, adopting a circular economy and lean management for renewable energy can reduce emissions and pressure on natural resources, chart innovative pathways to net-zero economies, create sustainable economic growth and jobs, and diminish supply chain risk. Considering the strong competition between industries worldwide, it is important to ensure quality, control costs, and improve production technology, thus appearing the concept of lean manufacturing which focuses on reducing costs while maintaining quality, minimizing waste generation, and enhancing customer satisfaction [4].

The circular economy is a sustainable economic model that prioritizes resource efficiency by minimizing waste and promoting the reuse and recycling of materials. This approach reduces the demand for new raw materials, which, in turn, decreases the energy and emissions associated with their extraction and processing. By designing products for longevity and recyclability, the circular economy significantly cuts down on waste, lowering landfill emissions and the overall carbon footprint linked to waste management. Additionally, it encourages the adoption of sustainable production processes that utilize renewable energy and greener technologies, contributing further to reduced greenhouse gas emissions.

Moreover, the circular economy fosters innovative business models, such as product-as-a-service, which shift consumer behavior towards sustainable choices, like purchasing second-hand goods. This not only decreases the demand for new products but also encourages collaboration across industries to innovate and close material loops, driving down emissions throughout supply chains. By integrating circular economy principles, we can

enhance carbon sequestration through improved land use and forestry practices, ultimately supporting the goal of achieving net-zero emissions while creating economic opportunities and resilience in an evolving world.

Non-conventional energies are based on durable materials whose properties prove their efficiency in applications. For these materials, strength and durability must be high, to present exceptional mechanical properties, including high fracture toughness and wear resistance. Thus, the manufactured products will have a long lifespan, reducing the need for frequent replacements and thus minimizing waste, an aspect that aligns with the principles of the circular economy and lean manufacturing. In addition, to ensure the longevity and reliability of the products, the materials used must show chemical stability and be inert, allowing them to be used in harsh environments, without degradation.

Materials used in the structure of energy storage devices can accumulate more energy from the environment than they consume, allowing for sustainable operation. This advantage has led to the creation of portable energy collection systems that can contain, for example, 2D materials, which have a high surface-to-volume ratio [5]. Recently reported sustainable materials that go into energy storage are hemp-derived electrodes [6] and honeydew peel-derived carbon [7]. Among the different energy conversion and storage systems, ceramic materials represent an alternative in the design of these systems due to their high-power density, excellent thermal stability, long lifespan, and environmental friendliness [8].

Zirconia is a polymorphic material occurring in three temperature-dependent crystallographic arrangements: the monoclinic phase (m), thermodynamically stable from room temperature to 1170 °C; the tetragonal phase (t), stable from 1170 to 2370 °C; and the cubic phase (c), stable from 2370 °C to the melting point [9]. The most important phases for engineering are the tetragonal and cubic phases [10]. These phases can be achieved through high-temperature heat treatment, incorporation of lower-valence dopant metals into the crystal lattice, like CaO, magnesia (MgO), and yttria (Y_2O_3) [11], or by increasing the surface energy of nanoparticles [12]. The alloying induces the formation of oxygen vacancies or reduces the crystallite size [13]. Stabilizing the tetragonal phase at room temperature is crucial to harness its transformation toughening properties [14]. Without stabilization, the phase would revert to being monoclinic, leading to potential failure under stress and thermal degradation. When ZrO_2 contains a mixture of both tetragonal and mono-clinic phases within its matrix, it is referred to as partially stabilized zirconia (PSZ). In contrast, if ZrO_2 is primarily composed of the tetragonal phase, it is called tetragonal zirconia polycrystals (TZP) [13]. During cooling from high processing temperatures to room temperature, a spontaneous stress-induced martensitic transformation from the tetragonal (t) to monoclinic (m) phase can occur, which restricts the use of pure ZrO_2 as an advanced structural material. It is well established that controlling the crystal phase is essential to meet the optical requirements of zirconia applications. Fujii et al. [10] successfully developed genetic algorithm optimized potentials (GAOPs), which accurately reproduce the stability of various ZrO_2 structures, including monoclinic, tetragonal, cubic, orthorhombic I and II, as well as other hypothetical phases. To serve as a high-performance ceramic material, ZrO_2 needs to maintain its high-temperature cubic phase at room temperature [15]. The cubic phase zirconia is a promising material for applications as solid oxide fuel cells (SOFC), electrochemical capacitor electrodes, and oxygen sensors [16] due to the high electrical conductivity [13]. Cubic zirconia, in particular, has evolved as a viable alternative to diamonds (which are extremely expensive). Aside from its durability and strong aesthetic similarity to diamond, cubic zirconia produces cuts unlike diamonds and has optical flawlessness that appears completely colorless to the naked eye [17].

In this materials class, zirconia (zirconium dioxide, ZrO_2) has gained a special interest in the last period, considering its versatility and durability as a material with applications in non-conventional energy. Due to its advanced properties, ZrO_2 has various applications where its sustainability has been proven.

The main properties and applications of ZrO_2 are illustrated in Figure 2.

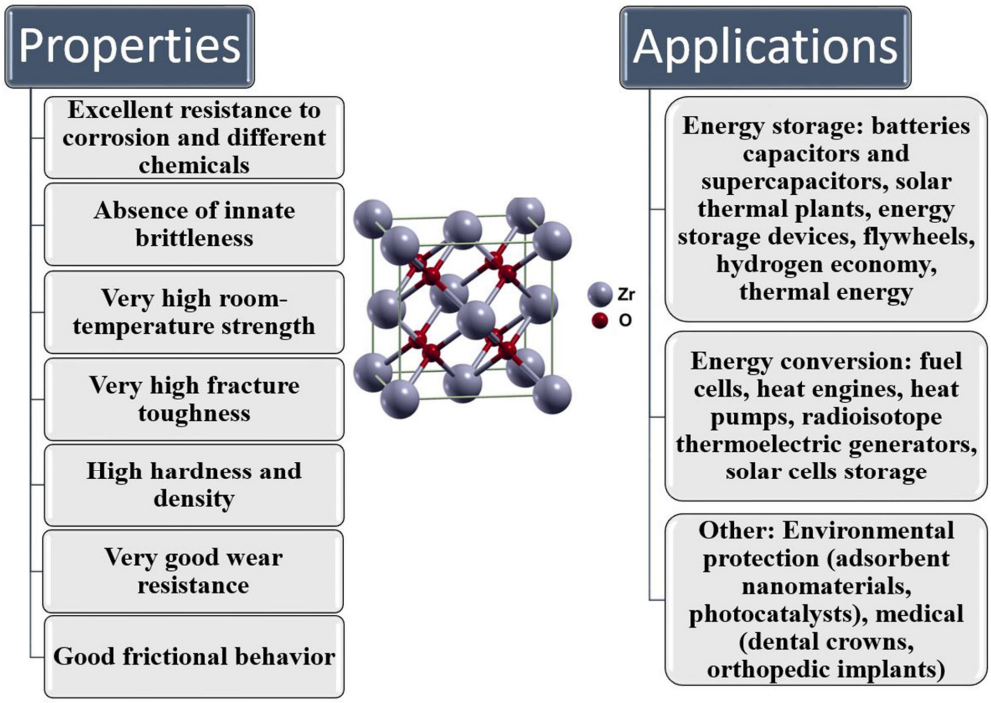

Figure 2. Properties and applications of ZrO_2 materials.

For example, zirconia's biocompatibility and durability make it a preferred material for dental crowns [18], catalysis [19,20], coatings as thermal barriers [21,22], and in display and photonic devices [23,24] owing to its short-wavelength luminescence properties. These medical applications benefit from ZrO_2's long lifespan, reducing the frequency of medical procedures and associated waste [25]. ZrO_2 is also used in high-performance components in the automotive and aerospace industries due to its high-temperature stability and wear resistance. These applications contribute to the efficiency and longevity of engines and other critical systems [26]. Additionally, ZrO_2 is used in catalysts and membranes for environmental applications, including air and water purification. Its role in these applications helps to reduce pollution and improve environmental quality [27–30]. In the energy sector, ZrO_2 is used in solid oxide fuel cells (SOFCs) and thermal barrier coatings for turbines [31–33]. These applications enhance energy efficiency and contribute to the development of cleaner energy technologies. The use of ZrO_2 in high-temperature and high-stress environments further enhances energy efficiency and extends the longevity of industrial processes and equipment [34].

The above considerations allow ZrO_2 to be a sustainable material due to its use in applications that contribute to environmental protection, energy efficiency, and long-term reliability. Additionally, its recyclability and relatively low environmental impact reduce the need for the extraction and processing of raw materials.

2. Synthesis Methods

Nano-ZrO_2 finds widespread application across numerous industries and research fields, and it can be synthesized through various methods. Each synthesis approach can be tailored to produce nano-ZrO_2 with specific performance characteristics. Obtaining nano-ZrO_2 is based on two alternatives: top-down and bottom-up approaches, as presented in Figure 3.

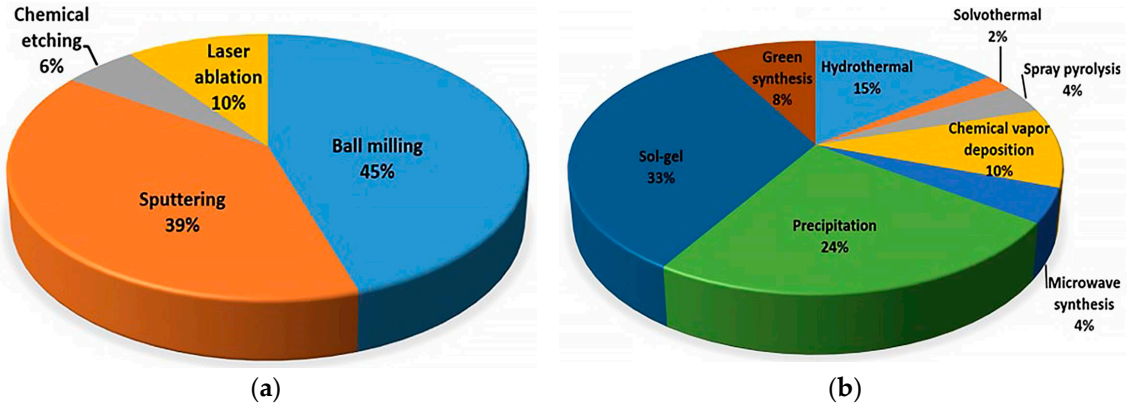

Figure 3. Number of publications in Web of Science core collection regarding ZrO_2 preparation methods: (**a**) top-down approaches, (**b**) bottom-up approaches.

The top-down approach involves using bulk material to obtain crystallites by controlling the processing parameters through physical methods. However, this can produce intermediates, and achieving a nanometric size can be more difficult compared to the bottom-up approach [35]. Through the bottom-up approach, using physical and chemical methods is effective, but can be ecologically polluting. In contrast, biological methods that use plants, fungi, algae, and bacteria offer ecological benefits and sustainability [36,37]. The methods used to obtain ZrO_2 usually involve work protocols that include chemical synthesis and, thus, a risk for the environment, so the biological methods applied in manufacturing nano-ZrO_2 for solar cells must become a viable solution for the future [38]. This section provides a detailed comparison of the different synthesis methods used to fabricate nano-ZrO_2. Over the past 20 years, ZrO_2 has been studied for various applications, from bone implants to catalysts and fuel cells, due to its biocompatibility, corrosion resistance, temperature stability, and hardness. Nano-ZrO_2 exhibits improved physico-chemical properties due to its reduced particle size and increased specific surface area. Recent innovations in the synthesis of nano-ZrO_2 have led to new applications with superior performance and a wide range of morphologies controlled by synthesis parameters such as temperature, pH, and reaction time. In addition, recent green and large-scale synthetic processes have gained attention, with an emphasis on cost-effective and environmentally friendly synthetic routes utilizing alcohols. Studies have demonstrated that nano-ZrO_2 with varied morphologies and sizes can be synthesized using several methods. These morphologies include nanoparticles, nanorods, nanotubes, nanowires, nanosheets, and mesoporous structures, all of which can be controlled by varying the working parameters, such as temperature, pH, and reaction time [39]. This progress in the synthesis of nano-ZrO_2 is highly relevant to researchers in various fields, including materials science and chemistry, and enables the industrial production of high-quality and low-cost nano-ZrO_2.

2.1. Top-Down Approaches

2.1.1. Ball Milling Method

Several methods are used for the preparation of ZrO_2-based materials, like sol-gel, precipitation, hydrothermal, and ball milling. Compared to the other methods, ball milling does not require the use of solvents, high temperatures, or long-term reaction times [40]. This method is fast and can be done at ambient temperature, allowing good control over the microstructure (shape, size, etc.), leading to homogenous materials with a high-purity crystalline phase [41]. The literature reports promising results from grinding with a ball mill to obtain t-ZrO_2 from m-ZrO_2, with the transition to the tetragonal form reaching about 45% in 50 h. Both tetragonal and monoclinic crystallites are about 10 nm in size. As a rule, to increase the transition to the solid phase, doping with Y_2O_3, Fe_2O_3, and CoO oxides (6–10% by weight) is employed [42]. The use of a high-energy planetary ball mill can lead to the disintegration of the particles into crystallites as small as 20 nm, facilitating

a rapid transition to the solid phase. Macan et al. [43] reported the performance difference between Al_2O_3 doped Y_2O_3 stabilized ZrO_2 prepared by two methods: ball milling and sol-gel. They found that the ball milling method yielded materials with homogenous morphology, whereas the samples prepared by the sol-gel method presented a tetragonal phase. This correlates with previous findings that demonstrate mechanical ball milling leads to materials with improved shape and dispersion.

While ball milling presents several advantages, it also has some limitations, for example, the equipment can be heavy and cumbersome, leading to handling challenges, while the process consumes considerable energy due to wear, friction, and heat generation [44]. Furthermore, it can generate contamination and noise, complicating the maintenance of material purity and workplace comfort. Thus, while ball milling is a powerful technique in material processing, these drawbacks must be carefully considered in its application.

2.1.2. Sputtering Method

Sputtering is a physical process known as physical vapor deposition (PVD), which is characteristic for the fabrication of thin films. Spraying takes place in a vacuum and is suitable for metals, textiles, or other materials where control regarding the thickness of the layer is essential. An elementary target is used in a gaseous atmosphere to form the desired compound, and the deposition rate depends on the gas flow rate and partial pressure [45]. ZrO_2 films, which can be approx. 75-nm thick, can be deposited on silicon and quartz substrates via the reactive Direct-Current (DC) magnetron sputtering of the zirconium target [46]. In a study by Verma et al., nano-ZrO_2 was prepared by the reactive magnetron sputtering technique using various sputtering power [47]. The NPs obtained presented a tetragonal structure with an increased average crystallite size from 3 nm to 8 nm, with an increase in sputtering power from 40 W to 100 W, as can be seen in Figure 4.

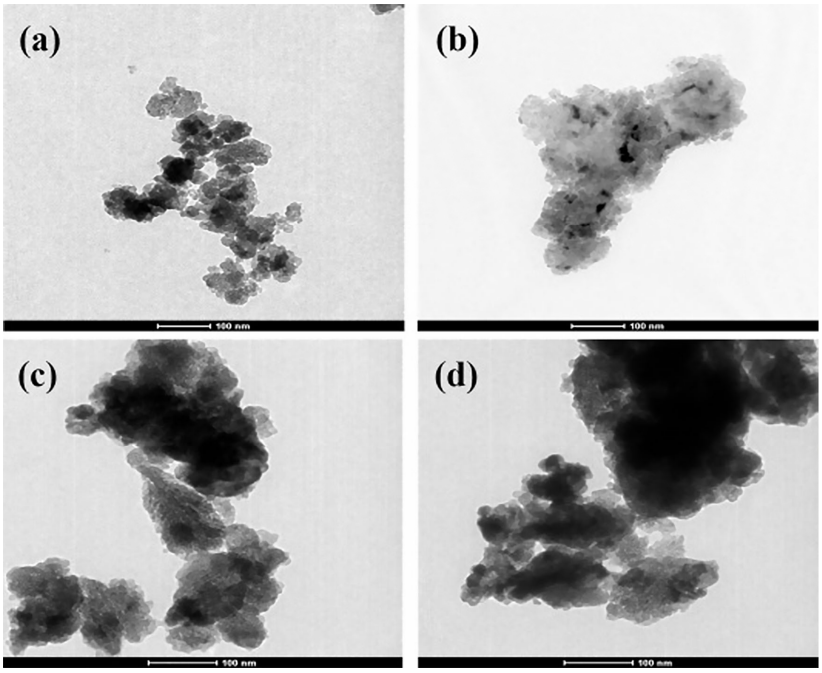

Figure 4. TEM images of ZrO_2 nanoparticles synthesized at (**a**) 40 W, (**b**) 60 W, (**c**) 80 W, and (**d**) 100 W sputtering power. Reprinted with permission from [47].

Patel et al. suggested that Ar partial pressure influences the band gap and refractive index of ZrO_2 thin films [48]. They found that, with the increase in Ar partial pressure, the thickness of the ZrO_2 films decreased from 433 nm to 385 nm, leading to an increase in band gap from 4.28 eV to 4.46 eV. Also, the average crystallite size increased from 19 nm to 25 nm.

Some of the advantages of this method include low operating temperatures, providing a stable, long-lived vaporization source, and it can coat large areas more uniformly. However, it also presents some limitations, like lower deposition rates compared to thermal evaporation, lower material purity, and the high cost of the necessary equipment [44].

2.1.3. Chemical Etching Method

One of the top-down approaches is chemical etching that is applied for ZrO_2. This method presents a challenge due to the wet etching resistance of ZrO_2. As a rule, diluted HF is used, along with H_2SO_4, HCl, and H_3PO_4 for the wet etching of semiconductors based on metal oxides to remove the dielectric in the open source and drain regions [49]. HF remains most efficient at concentrations between 0.1 and 0.5%, but its effectiveness decreases when the formed fillets are subjected to heat treatment [50]. For high efficiency, the onset temperature of crystallization is important, which, as it increases, causes a transformation from tetragonal to monoclinic phases in the films. The addition of fluorine or neutral species such as silicon can increase the effectiveness and selectivity of wet chemical etching, making it the most feasible way to obtain improved burn speeds. The trend in metal oxide semiconductors is to use SiO_2 with high-k dielectrics (high dielectric constant), such as TiO_2, Ta_2O_5, ZrO_2, Y_2O_3, La_2O_5, HfO_2, aluminates, and silicates. A method for the wet chemical etching of hafnium and zirconium oxides to obtain a layer of Hf or Zr oxide material over a silicon dioxide layer is described in the literature. This involves the use of a wet etching solution consisting of a solvent mixture (H_2O, $HClO_4$, alcohol, tetrahydrofuran (THF), sulfuric acid (H_2SO_4) and dimethyl sulfoxide (DMSO)) and a halogen-containing acid (HF, HBr, HI, and $HClO_4$). The purpose is to achieve an etch rate relative to the material layer of about 2.5 times higher than an etch rate of silicon dioxide [51].

2.1.4. Laser Ablation Method

Laser ablation is an efficient method for thin film deposition and the micromachining of metals, ceramics, and polymers. One advantage is the possibility of high-speed heating and quenching of materials, leading to the form of metastable phases in the target. For example, metastable cubic ZrO_2 can be formed by an ultraviolet laser ablation reaction occurring from zirconium atoms in an oxygen atmosphere at room temperature and 1.5 mbar [52]. Many studies have reported the use of the laser ablation method in the preparation of ZrO_2 materials. The synthesis of single phase (cubic) ZrO_2 in ammonia and mixed phases of ZrO_2 (monoclinic and tetragonal) using pulsed laser ablation (PLA) in water was reported by Tan et al. [53].

Laser ablation in an oxygen reactive atmosphere (10^{-3}–0.1 mbar) was employed for the formation of ZrO_2 thin films with a thickness of 200–500 nm [54]. The study showed that the optimal surface morphology was obtained by ablation of a Zr target at a fluency of 6 J/cm^2 in an O_2 atmosphere at a pressure of 5×10^{-2} mbar. The dielectric constant was measured to be between 12 and 24 across a broad range of frequencies (20 Hz to 2 MHz) and temperatures (20 to 150 °C).

Some of the major advantages of the laser ablation method are lower energy loss and the generation of ligand-free NPs in a range of solvents [55]. This method also presents some drawbacks, like the ablation effectiveness drops with increased ablation duration, and on an industrial scale the most dispersed laser sources are incapable of creating NPs.

2.2. Bottom-Up Approaches

2.2.1. Hydrothermal Method

The hydrothermal method is extensively employed for synthesizing nano-ZrO_2 because it enables precise control over synthesis parameters, resulting in nano-ZrO_2 with tailored properties. The synthesis methods and thermal treatment decide the crystallinity and properties of nano-ZrO_2 [56]. This technique integrates physical parameters like pressure, temperature, and time with chemical reactions involved in nanoparticle formation. Commonly used for synthesizing ceramic powders, it operates under high temperatures

and pressures within a liquid medium. Furthermore, the method facilitates the incorporation of dopants, modifiers, and surfactants, making it excellent for the large-scale production of nano-ZrO_2 [39].

Hydrothermal synthesis is based on chemical reactions in aqueous or organo-aqueous solutions, which take place at temperatures above 100 °C and pressures above 1 atm, in an alkaline or acid environment with a pseudo-catalytic role [57]. The advantage of this method is the possibility to control the particle size and obtain pure compounds at low temperatures through various reactions including hydrolysis, coprecipitation, oxidation, and decomposition [57]. With regard to the size control, ZrO_2 particles resulted in an average size of 15–30 nm, and could have about 72% cubic or tetragonal phases, and a 28% monoclinic phase. The cubic phase allows high oxygen ionic conductivity and stability in nano-ZrO_2, offering the potential for different applications such as oxygen sensors, solid oxide fuel cells, and catalysts [57].

2.2.2. Solvothermal Method

The solvothermal method is similar to the hydrothermal method, with the difference that the reaction medium is a solvent, rather than water, while maintaining the same temperature and pressure conditions. It is considered a physico-chemical method that ensures a good solubility of the precursors and allowing rapid homogeneous reactions [39]. Some of the main issues of solvothermal synthesis are crystal structure, crystallinity, shape control and arrangement, and particle size distribution [58]. The process can lead to different particle morphologies such as spherical, nanofilms, nanorods, nanosheets, and nanowires [59]. Recent advancements in the field have demonstrated that integrating external fields such as microwaves, ultrasound, or mechanical stirring into the solvothermal process can significantly enhance the quality of nanoparticles produced [60]. For example, a microwave–solvothermal method was used by Mishra et al. to produce t-ZrO_2 nanoparticles with the size of 10 nm, using $ZrO(NO_3)_2$ and 1,4-butanediol [61]. In another study, ZrO_2 NPs with a diameter of 4 nm were synthesized using the microwave-assisted decomposition of zirconium acetate in the ethoxyethanol [62].

Another crucial element in the solvothermal method is the chemical environment. The morphology and stability of the final NPs can be influenced by a number of variables, including the reaction medium's pH, the precursors' chemical composition, and the additive selection [63]. In order to control particle growth and achieve the desired qualities, additives—which might include biomolecules, surfactants, and polymers—act as capping agents or structure-directing agents.

In terms of precursors, both organic and inorganic options are utilized in solvothermal synthesis. Organic precursors like zirconium acetate and zirconium alkoxide, alongside inorganic ones like zirconyl chloride and zirconyl nitrate, can lead to the formation of different ZrO_2 phases under similar conditions [64]. Research has confirmed that varying the precursor type can result in distinct crystal structures, such as cubic or monoclinic zirconia, further highlighting the versatility of the solvothermal approach. Keukeleere et al. [65] proved in their study that monoclinic ZrO_2 was synthesized from ethoxide, while cubic ZrO_2 can be obtained via acetate, ethoxide, or propoxide precursors. Ionic liquids have also emerged as promising media for solvothermal synthesis, owing to their unique physicochemical properties [66]. These liquids can provide excellent solubility for precursors and exhibit good thermal stability, making them suitable for producing inorganic and hybrid materials. For instance, researchers have successfully synthesized zirconia nanowires using zirconium tetra-n-propoxide in conjunction with an ionic liquid, achieving well-dispersed nanostructures with a length of 20 μm and a diameter of 50 nm [67].

2.2.3. Spray Pyrolysis

Pyrolysis by spraying involves two processes: one physical, spraying, and another chemical, pyrolysis. By spraying a precursor solution at high temperatures on a substrate based on chemical reactions, a thin film is formed whose thickness and uniformity can be

controlled. The method is suitable for large applications [39,68]. Hwangbo et al. combined a citrate precursor technique with salt-assisted ultrasonic spray pyrolysis to develop t-ZrO_2 NPs with an average diameter of 10 nm [69]. In their study, Mangesh Waghmare et al. reported the use of a zirconyl chloride octahydrate precursor at different concentrations to deposit thin films of c-ZrO_2 on a glass substrate at 450 °C. They observed that the particle size was lower than 20 nm, and also observed an increase in the optical band gap and in the crystallinity values of the deposited zirconia films with the increase in precursor concentration [70]. Chen et al. studied the influence of precursor solubility on the morphology of spherical ZrO_2 produced via ultrasonic spray pyrolysis [71]. They concluded that a gas-to-particle conversion mechanism results in smaller particle sizes compared to the one-particle-per-drop mechanism. Another study by Muelle et al. focused on synthesizing ZrO_2 NPs (80–95 wt% tetragonal phase) using flame spray pyrolysis at high production rates (up to 600 g/h) [72]. They utilized zirconium n-propoxide diluted in ethanol, leading to average particle diameters of 6–35 nm, influenced by dispersion gas flow rates and precursor concentrations.

While spray pyrolysis is an effective method for synthesizing ZrO_2 NPs, it also has its limitations. The equipment can be complex and costly, requiring the precise control of parameters like temperature, pressure, and precursor flow rates. It can be challenging to achieve uniform particle size and morphology, as variations in these parameters may lead to inconsistent results. Additionally, scaling up the process for industrial applications can pose difficulties in maintaining quality and efficiency. The use of solvents in precursor solutions complicates the process and raises potential environmental concerns, necessitating solvent recovery systems.

2.2.4. Chemical Vapor Deposition

The chemical vapor deposition (CVD) method is considered a physico-chemical process through which gaseous vapors are deposited in the form of a thin film on a surface, based on chemical decomposition and deposition reactions. This method is rarely used in industrial applications [73–75]. The CVD method has been widely reported in the literature for the preparation of nano-ZrO_2. By using $Zr(OBut)_4$ as a precursor, Hemmer et al. obtained microporous nano-ZrO_2 membranes on the surface of Al_2O_3 substrates by one-step liquid-injection CVD [76]. Based on the process parameters used, the morphology and roughness varied, obtaining a mixture of monoclinic and tetragonal phases at 500 and 600 °C. Another study reported the synthesis of ZrO_2 nanowires from $ZrCl_4$ powder at 1200 °C under 760 Torr on a graphite substrate with a pre-deposited thin layer of gold as a catalyst [74]. The study indicated that the nanowires formed at higher temperatures were longer, larger, and exhibited greater size variation (120–160 nm at 1100 °C—Figure 5a and 200–800 nm at 1150 °C—Figure 5b).

Kim et al. [77] synthesized ZrO_2 thin films via metal-organic CVD with ultrasonic nebulization, using various zirconium compounds as precursors at temperatures between 300 and 550 °C. They observed that higher substrate temperatures resulted in larger grain sizes, with an optical energy band gap of 5.32 eV. Films deposited below 450 °C were primarily monoclinic, while those above 450 °C exhibited a tetragonal structure.

The CVD method offers several advantages for various applications, but it also has notable disadvantages [78,79]. The need to transfer material from deposited substrates for additional assessment is one problem that might make procedures more difficult. The higher production costs are another major disadvantage. Certain precursors employed in CVD can be highly costly, while others are poisonous, flammable, or explosive. Additionally, several CVD process changes may result in increased fabrication costs. The kinds of substrate that can be employed are additionally restricted by the high deposition temperatures that many CVD techniques need. Lastly, the procedure produces extremely hazardous gaseous byproducts, which raises additional safety and environmental issues.

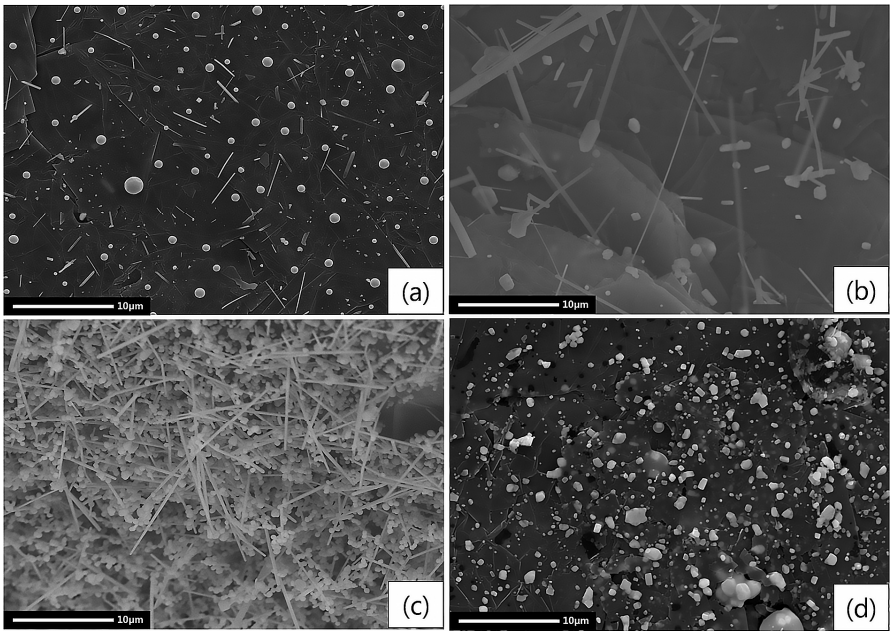

Figure 5. SEM images of zirconia nanostructures grown with Au catalyst at (**a**) 1100 °C, (**b**) 1150 °C, (**c**) 1200 °C, and (**d**) grown at 1200 °C with no Au catalyst. Reprinted with permission from [74].

2.2.5. Microwave Method

The microwave irradiation method uses the physical effect of the energy on molecules, providing fast and efficient heating for the rapid obtention of nano-ZrO_2. The advantage of this method is the control over the synthesis process and, thus, the establishment of the kinetic mechanisms and the product's characteristics, but without the possibility of scaling at the industrial level [39,80]. Because the microwave method requires less processing time, low power consumption, and generates uniform products, it has been widely used in ceramics production. ZrO_2 NPs were obtained from zirconium acetate hydroxide and distilled water solution which was subjected for 6 min to a 2.45 GHz frequency at 800 W power, resulting in NPs with sizes between 7 and 14 nm [81]. In a study by Hoffmann et al., a RAGA's microwave system was used on a zirconium oxychloride octahydrate and NaOH solution at 80 °C, 420 W, and 12 min. After calcination for 2 h in air atmosphere and 400 °C, both m-ZrO_2 and t-ZrO_2 were obtained with particle sizes lower than 10 nm, as presented in Figure 6 [82].

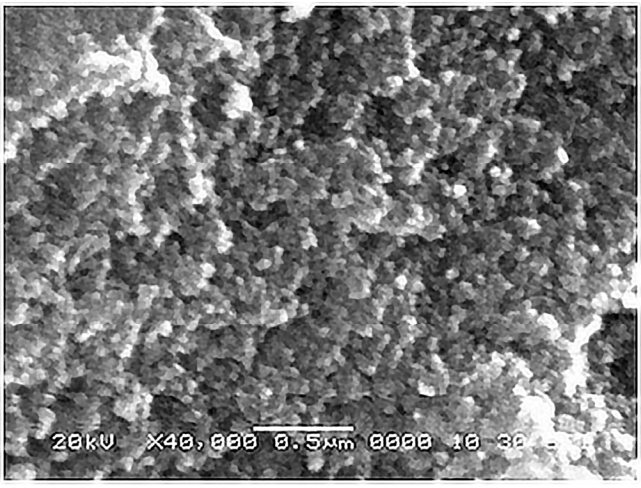

Figure 6. SEM micrographs of ZrO_2 NPs [82] (open access).

In another study performed by Manjunatha et al., zirconyl nitrate monohydrate, deionized water, and amino acid were used to synthesize ZrO_2 NPs. The gel obtained was irradiated for 60 sec at 800 W power, leading to NPs with a cubic structure and spherical morphology, and particle sizes between 60 and 65 nm [83].

2.2.6. Precipitation Method

Precipitation synthesis is the easiest method to obtain nanoparticles, by forming a $Zr(OH)_4$ in an alkaline medium (pH 10), followed by its calcination until it crystallizes in the form of Zr oxide [84]. Depending on the precipitation conditions, pH, and crystallization temperature, three ZrO_2 phases can form: cubic (c-ZrO_2), monoclinic (m-ZrO_2), and tetragonal (t-ZrO_2). For example, the formation of t-ZrO_2 takes place at 390–400 °C, and by increasing the temperature to 700 °C, m-ZrO_2 is formed. The porosity of the obtained material is very important in practical applications. In processes such as photocatalysis, the phase type and purity influence the band gap energy, which provides high efficiency in the process [85]. The co-precipitation method, as a method derived from precipitation, also represents a simple means of the simultaneous precipitation of zirconium ions with hydroxide ions. It also allows for the control of pH, temperature, and reaction time, which provides adequate control over the particle size, morphology, and crystal structure of nano-ZrO_2 [39].

2.2.7. Sol-Gel Method

The sol-gel method is a common synthesis method for nano-ZrO_2, offering the advantage of large-scale application with adequate control over particle size, morphology, homogeneity, crystalline structure, and composition. This method is based on the hydrolysis and condensation reactions of the precursor molecules to form a gel that led to nano-ZrO_2 through thermal processing, as observed in Figure 7.

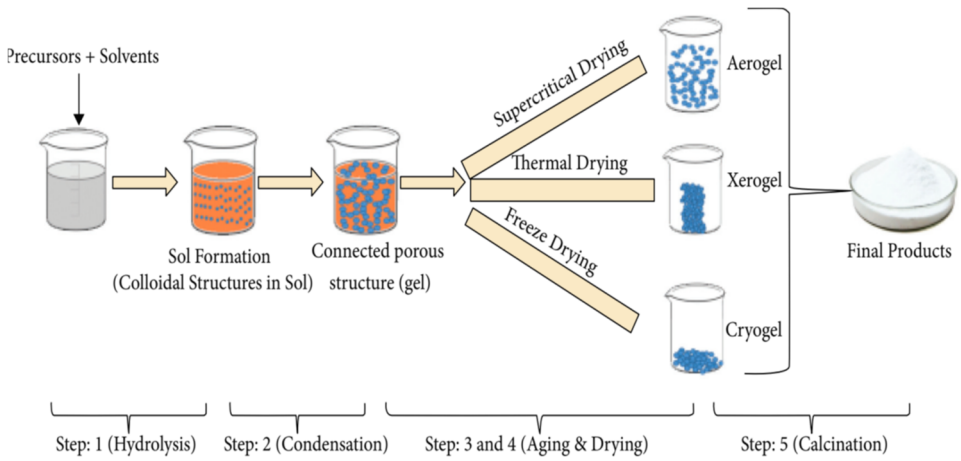

Figure 7. An overview of the steps of the sol-gel method. Reprinted with permission from [39].

Many studies have reported the use of the sol-gel method for the synthesis of nano-ZrO_2 [86–88]. A study by Ordóñez et al. reported the effects of anionic, cationic, and non-ionic surfactants on the stability and dispersion of nano-ZrO_2. They found that surfactants improved stability and reduced agglomeration. Their process involved mixing 5.4 mL of zirconium isopropoxide (IV) with 78.8 mL of 2-propanol, adding acetic acid, and then deionized water dropwise. The TEM analyses showed that, after stirring and drying, the gel was calcined at 800 °C, resulting in particle sizes of 59.9 nm ± 13.5 nm (Figure 8) [89].

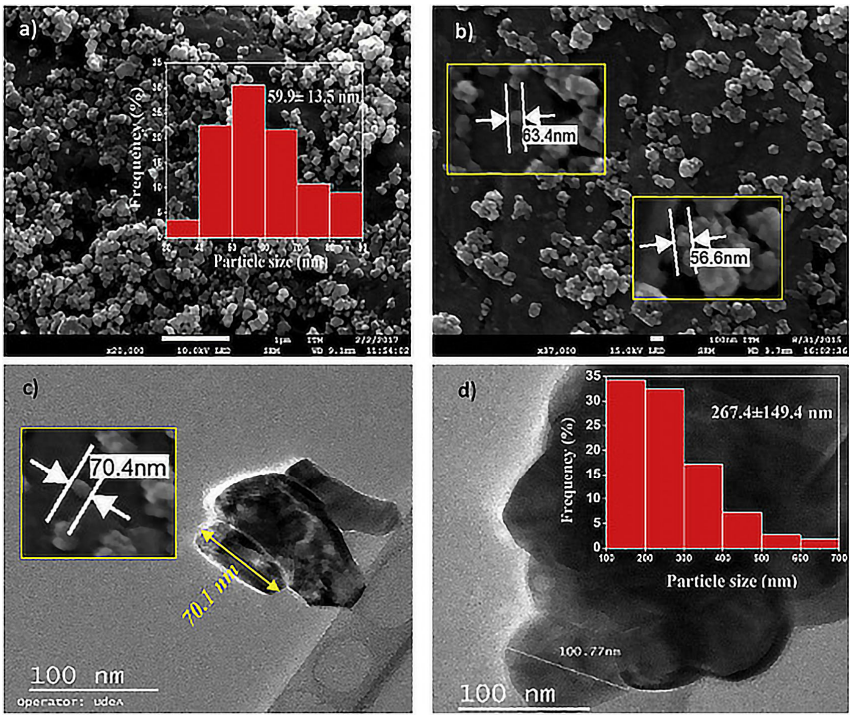

Figure 8. (**a**,**b**) FE-SEM and (**c**,**d**) TEM images of the sol-gel synthesized ZrO_2. Inset: histogram of particle size distribution. Reprinted with permission from [89].

The effect of pH on optical, morphological, photocatalytic, spectral, and structural properties was investigated by Dharr et al. [90]. Their findings showed that, with an increase in pH, the bandgap values increased and the crystallite size decreased. Waghmare et al. studied how annealing temperature affects the structural and optical properties of nano-ZrO_2. They synthesized nanocrystalline ZrO_2 by mixing zirconyl chloride octahydrate, ethylenediaminetetraacetic acid (EDTA), and ammonium hydroxide, then drying the gel. The resulting material was annealed at 650 °C, 750 °C, and 850 °C for 2 h to produce crystalline ZrO_2 nanopowders. Their results indicated that crystallite size varied with annealing temperature, and that with increased temperature the UV–Vis absorption band edge decreased [91].

Self-assembly chiral low-molecular-weight gelators (LMWGs) were used as templates by Huo et al. [92] to prepare left- and right-handed helical ZrO_2 nanotubes and double-coiled nanoribbons with outer dimensions of 300–700 and 800 nm.

The sol-gel method offers several advantages, making it a popular choice for synthesizing materials [44,93]. It is cost-effective and produces homogeneous materials with high purity. Additionally, it operates at low processing temperatures, which is beneficial for creating composites and complex nanostructures. The method also allows for the uniform introduction of small amounts of dopants into the sol, ensuring even distribution in the final product. However, there are some disadvantages to consider [94,95]. The reaction time can be longer compared to other methods, and the use of organic chemicals poses health risks. Furthermore, samples often require post-treatment for purification, which can add to the complexity of the process.

2.2.8. Electrochemical Deposition

Electrochemical deposition is a method used for the fabrication of nanostructured films that present some significant advantages like high deposition rates and good control over the thickness of the deposited film with high purity and uniformity [96]. The literature reports many studies that used electrochemical deposition to obtain a ZrO_2 coating over different substrates like AISI 316L stainless steel [97,98], commercial titanium [99], boron-doped diamond electrodes [100], and NiTi alloys [96,101]. The mechanism for the formation

of ZrO_2 from aqueous electrolytes of zirconyl salts usually implies the electrosynthesis of zirconium hydroxide particles on the surface of the substrate. At first, the dissolution of salts in water leads to the formation of zirconyl cations (ZrO^{2+}) that are solvated, leading to the formation of the tetramer $(Zr_4(OH)_8(H_2O)_{16})^{8+}$, a solution that is highly acidic due to the tendency of these solvated species to release protons [102]. The pH level increases near the cathode surface during the cathode reactions that take place during the electrodeposition process, causing colloidal zirconium hydroxide particles to precipitate on the substrate surface. In the next step, this hydroxide undergoes dehydration, resulting in the formation of ZrO_2 [96].

2.2.9. Atomic Layer Deposition (ALD)

In contrast to PVD and CVD processes, atomic layer deposition (ALD) is an alternative technique that allows the deposition of highly uniform and conformal films on substrates of any shape at low temperatures, offering precise control over film thickness at the atomic level [103]. The nature of the precursor used plays a critical role in the growth per cycle (GPC), crystallinity, and temperature range for the deposition of ZrO_2 films. Many studies have reported the use of the ALD process in the development of ZrO_2 by using different precursors like $Zr(OC(CH_3)_3)_4$ [104], $ZrCl_4$ [105], and ZrI_4 [106]. There are advantages and disadvantages for each precursor used in the process. $ZrCl_4$ presents low volatility and requires a high evaporation temperature in the ALD process [107]. Also, by using $ZrCl_4$ and H_2O in the ALD process, HCl is generated, leading to corrosion risks and the degradation of the ZrO_2 film [108]. Frequently utilized precursors include alkylamido- and cyclopentadienyl-based compounds, such as $Zr(NMe_2)_4$, $Zr(NEtMe)_4$, and Cp_2ZrMe_2 (Me—methyl, Et—ethyl, and Cp—cyclopentadienyl) [109]. However, alkylamido ligands tend to exhibit low thermal stability, and the GPC for Cp precursors is lower than that of alkylamides. Another precursor investigated that presented high reactivity to surface ligands (e.g., -OH), high volatility, and good thermal stability is 3 tetrakis(dimethylamido)zirconium(IV) ($Zr(NMe_2)_4$ or TDMA-Zr). Liu et al. investigated the use of this precursor and H_2O for the formation of ZrO_2 films on nitrogen-doped carbon nanotubes (N-CNTs) [110] and graphene nanosheets (GNS) [111]. They concluded that thin films can be obtained at temperatures lower than 100 °C, with crystallinity and GPC strongly depending on the deposition temperature.

2.2.10. Green Methods

Green methods involve physical, chemical, and biological methods that have the advantage of eliminating the consumption of reagents that negatively affect the environment. A comprehensive overview of green methods for nano-ZrO_2 synthesis was suggested by Van Tran et al. [35], as presented in Figure 9.

Green synthesis can be achieved with the help of plants or microorganisms (bacteria, fungi, or algae). Plants are a locally available resource and are advantageous for large-scale applications. Compared to other green materials such as bacteria, fungi, and algae, plant use reduces the microbial risk by avoiding the secretion of metabolites or toxins during cultivation and use [35]. The reaction time is faster and the kinetic speed is higher in the production of nano-ZrO_2, with biomolecules in the plant performing the bioreduction of Zr ions in a few minutes. In contrast, microbial variants typically require several days under ambient incubation conditions [112]. Extracts containing biomolecules from plants are easy to obtain and control. The plant parts used can include leaves, bark, roots, or flowers, and the solvents are generally water or ethanol. Bacteria, the fastest-growing microorganisms, serve as efficient biofactories for the synthesis of nano-ZrO_2 under mild conditions of temperature, pressure, and pH. They can produce nano-ZrO_2 through bioreduction, biocapping, and biostabilization methods [35,113]. Also, there are various species of fungi that can be used in green synthesis, but specialized data have shown that algae, as predominantly aquatic organisms that use chlorophyll for photosynthesis, often yield superior results compared to terrestrial plants. Brown algae or marine algae

contain multifunctional polysaccharide-type biomolecules that can act as bioreducers for Zr ions forming nano-ZrO_2, with an average size of about 5 nm [114,115].

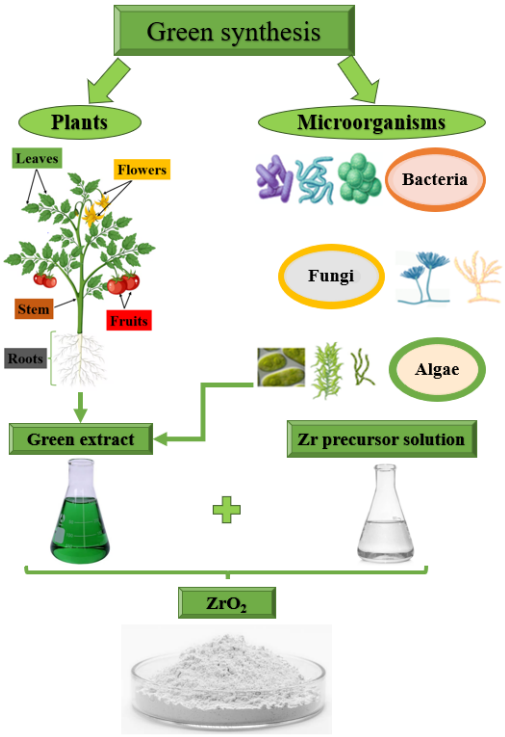

Figure 9. General representation of ZrO_2 green synthesis method.

Although recent innovative synthesis routes have enabled large-scale production, green methods are not yet feasible for industrial applications due to harsh environmental conditions for carrier survival, high energy consumption, and complex processes [39]. In the case of removing environmental pollutants, such as antibiotics and textile dyes, the issue of reusing ZrO_2 NPs must be addressed. For nano-ZrO_2-based nanocomposites, optimization of the biomass ratio is necessary to avoid interactions between the green extract and dopants. Additionally, the ecotoxicity of green-synthesized ZrO_2 NPs requires ongoing assessment. These limitations warrant further investigation [35]. Despite these limitations, the green synthesis of nano-ZrO_2 using microbial and botanical sources has attracted significant interest, as it offers several advantages, including eco-friendly and cost-effective production compared to traditional chemical synthesis methods [35].

3. Nano-ZrO_2 in Non-Conventional Energy Applications

Zirconium-based nanomaterials have been extensively researched and tested across various technological fields, demonstrating their effectiveness as fuel cells, sensors, catalysts, catalyst support, semiconductor devices, as well as in electro-optical, dielectric, piezoelectric, and structural applications [116–119]. Dopant-stabilized cubic zirconia can be synthesized through multiple methods, and its nanoparticles can be incorporated into electrolyte materials in fuel cells [120–125]. Zirconia is commonly utilized in ceramics due to properties such as a large band gap, low absorption, high melting point, and high dielectric constant. Nano-ZrO_2, stabilized at high temperatures, finds applications in dental implants, catalysis, and coatings as thermal barriers, and in display and photonic devices owing to its short-wavelength luminescence properties. Additionally, ZrO_2's non-toxic nature makes it an ecologically advantageous material, positioning it as a potentially highly functional material for future applications.

3.1. ZrO_2 as Advanced Material Support for Energy Conversion Systems

The use of electricity today is achieved through conversion from primary energy sources (fossil, nuclear, and hydro), but also from other non-conventional techniques, in which the solar cell, fuel cells, or batteries prove their applicability. The most important source of energy is sunlight that can be converted into electricity using solar cells. Today, local energy distribution networks are increasingly supplied by solar power plants. Batteries are used for both energy conversion and storage, with storage systems playing a key role in load balancing applications in power systems. Fuel cells generate electricity for a variety of applications, and, recently, energy generation has been explored through gas plasma or liquid metal effects that can move in a magnetic field. Additionally, thermoelectric and thermoionic conversion processes are being considered as potential applications in space vehicles [126]. The materials that form the basis for the development of such solutions are sustainable materials of the future, with ZrO_2-based matrices being successfully synthesized and tested. In renewable energy resource systems, solar cell technology offers the advantage of high-power conversion efficiency at low production cost.

Table 1 shows some examples from the last 10 years of methods of preparation and characteristics of ZrO_2 NP_s used in energy conversion applications.

Table 1. Significant examples over the past 10 years of publications regarding the preparation method and characterization of ZrO_2 with potential applications in energy conversion.

No.	Method	Characteristics	Year	Ref.
1.	Zirconium dioxide doped porous carbon nanofibers (ZrO_2-PCNFs) made by electro-spinning method	ZrO_2-PCNFs present high initial discharge specific capacity of 1003.2 mAh g^{-1} and maintains a capacity of 720.2 mAh g^{-1} after 400 cycles, with a decay rate of only 0.07% per cycle and conspicuous Coulombic efficiency of above 97.5%	2024	[127]
2.	ZrO_2 by precipitation method, calcination at different temperatures (50, 120, 150 °C), ZrO_2-1, ZrO_2-2, ZrO_2-3	ZrO_2-1: agglomerated particles (10–20 nm) as nanobars and nanospheres. ZrO_2-2: less agglomeration, 2–10 nm. ZrO_2-3 with 2–5 nm as nanosphere	2023, 2020	[116,120]
3.	ZrO_2-SiC hybrid nanofluid by mixing of ZrO_2 and SiC in distilled water as fluid and ultrasonication for a uniform suspension	Maximum thermal efficiency was 75.21% for 0.041 kg/s flow rate and 69.92% for 0.025 kg/s flow rate	2023	[128,129]
4.	ZrO_2 dopped with lanthanides oxides (Sm/Eu/Tm) by chemical co-precipitation and fabrication of thin films on ITO substrates by dip and spin coating	Lower bandgap energies i.e., 4, 3.88, and 3.57 eV for dopping method, crystallinity improvement from 67.92 to 45.23 nm		
5.	HfO_2/ZrO_2 nanolaminate thin films were deposited by thermal atomic layer deposition (ALD) at a substrate temperature of 280 °C	Total thicknesses of all the HfO_2 and ZrO_2 layers were 2.2 nm and 6.6 nm, adiabatic temperature change (ΔT) = 12.25 K	2022	[130]
6.	ZrO_2/(10–30 wt%)/Fe_2O_3 composites were produced by the powder metallurgy technology	Green compacts composites with cylindrical form, diameter of 13.7 mm, sintering at 1700 °C	2021	[131–133]
7.	Sulfur substitution on ZrO_2	Sulfur doping concentrations decrease the band gap from 3.1 eV (for the pure case) to 0.6 eV (for 14% of sulfur concentration)		
8.	Zr1-XMnXO NPs and Zr1-X FeXO NPs by coprecipitation method	Agglomerated granular and spherical shape, ZrO_2/Mn (1:1) with nanowire structure		
9.	TiO_2/ZrO_2 double electron transport layered perovskite solar cells	The energy conversion efficiency (ECE) increased initially with ZrO_2 layer thickness increase, reached a maximum ECE of 14.24% at 204 nm ZrO_2	2020	[134]
10.	ZrO_2–Y_2O_3 nanopowders were synthesized by a chemical technology of co-precipitation	ZrO_2–3% mol Y_2O_3 (particle size 7.5 nm) nanopowder	2019	[135]
11.	Co ferrite/ZrO_2 ceramic nanomixture synthesized by the propylene-oxide-assisted sol-gel method	Co ferrite/ZrO_2 ceramic nanomixture particle size ranging from 20 to 60 nm, specific surface area and pore volume decreased by 30.31 m^2/g and 0.0615 cm^3/g	2018	[136]
12.	ZrO_2–Y_2O_3 (3 mol%) via coprecipitation method	ZrO_2-Y_2O_3 (3 mol%) with an average particle size ~ 7.5 nm, compact material density is ρC = 3.1 g/cm^3, electrical energy (ΔU = 130 mV on a load of 1 MΩ)	2017	[137]
13.	Cubic Zr NPs via microwave combustion method	Mesoporous cubic ZrO_2 nanoparticles with sizes of 60–65 nm for the as prepared sample (MCZ-0)	2016	[83]
14.	ZrO_2 fibers were fabricated using the electrospinning method	ZrO_2-500 8.61 nm, ZrO_2-600 10.52 nm, ZrO_2-700 17.36 nm ZrO_2-800 19.36 nm ZrO_2-900 19.36 nm	2014	[138]

Today, metal oxide layers such as Al_2O_3, TiO_2, SiO_2, MgO_2, and ZrO_2 are used as energy barriers to restrict the recombination of charges [139–141]. ZrO_2 is a stable host material with good chemical stability and optical transparency in visible (VIS) and near infrared (NIR) regions. It also can be a good host for doping and energy transfer from ZrO_2 ions to rare earth ions such as Yb-3p, Er-3p, Tm-3p, Tb-3p, Eu-3p, and Ho-3p [132,142–144]. Also, sulfur doping nano-ZrO_2 improves its properties in photovoltaic applications, given that nanotechnology has focused, in recent years, on the development of semiconductor nanomaterials for solar cell applications [145–149]. Thus, ZrO_2 is an electron-carrying layer in solar cells, being, at the same time, a matrix for modifying the spectrum and photonic conversion. Doping ZrO_2 with 2p elements provides ferromagnet behavior at room temperature [150].

ZrO_2 can be a raw material for obtaining lead-free ceramic capacitors, which are critical energy storage components for advanced pulsed power systems, featuring ultra-high-power density and ultra-fast discharge speeds. Through the solid-state reaction, different ceramics can be obtained, with ferroelectric relaxor properties, including those based on $SrZrO_3$. This process enhances the fracture resistance by improving the electrical insulation and widening the band gap [151].

Through the unique properties specific to the active centers, nano-ZrO_2 functions both as a catalyst and support for the catalyst, having thermal stability and adjustable porosity, being able to attract and adsorb organic molecules and mediate organic reactions at high temperatures [116,152,153]. The ZrO_2 catalyst support has good stability against silica, alumina, and carbonate minerals, and is used in biodiesel synthesis, either alone or in combination with other active metals or metal oxides. Studies have reported increased efficiency when combined with alkali metals and sulfate ions for canola and soybean oils [154,155]. The catalytic activity depends on the acidity and/or basicity of the surface, the pore structure, and the specific surface. It also offers the possibility of reuse and recycling, which are important features in sustainable development from the perspective of the circular economy and lean management [156].

Oxide ceramics are considered promising absorbent materials with high efficiency and durability for the production of energy from solar radiation [131,157,158], with alumina (Al_2O_3) and zirconium (ZrO_2) being the most advantageous. As a rule, other dark materials such as Fe_2O_3 and MnO_2 are added to form new high-performance black composites [159]. The composites thus gain remarkable thermal, optical, and mechanical properties. Black ZrO_2/Fe_2O_3 composites have been studied for their efficiency and lifetime, characterized by concentrated solar radiation harvesting, zero emissions, and clean energy in the form of heat or electricity. Comparatively, superior properties, at low prices, were obtained for the Al_2O_3/CuO composite [160]. Silicon carbide (SiC) and aluminum nitride (AlN) composites, used in solar thermal power plants, also show high durability [159,161–163], but with high thermal emissivity and very expensive processing, when inert atmosphere is used to avoid oxidation [164].

In the case of materials for the solar receiver, the heat transfer can be inhomogeneous, leading to the formation of hot spots and potential damage [131,165]. Thus, the materials must be designed in such a way as to ensure good thermal conductivity and diffusivity [160]. This is the case with Al_2O_3/CuO and ZrO_2/Fe_2O_3 black composites, with maximum thermal conductivity values of 15.47 W/m K and 3.59 W/m K, respectively, both of which are poorly investigated.

Heat losses from the material surface are also very important, for which there should be low emissivity values in the infrared (IR) light, based on the emissivity evaluating the yield of the solar–thermal absorbent material [166–168]. Al_2O_3/CuO composites reach the emissivity value of 0.56, compared to ZrO_2/Fe_2O_3, which have a value of about 0.70 [131].

ZrO_2 can also be used in nano-fluid form as a heat-absorbing medium for solar flat panel water heaters (SPWH). The addition of nano-ZrO_2 with an average particle size of 50 nm in the aqueous environment led to a 20.68% increase in the efficiency of the heating system [169].

Renewable energy dominates at present due to its sustainability and ability to generate power on a large scale. Solar energy is notable for its popularity and rapid growth, although its performance is influenced by various factors [128,170–172]. Recent research has highlighted that nanotechnology brings added value to energy capture and storage systems. The incorporation of nanoparticles into fluids has considerably improved their properties, especially in solar thermal collectors, where an increase in the rate of heat transfer between the collector and the fluid has been observed due to higher thermal conductivity. Notable effects were observed when using a ZrO_2-SiC–water hybrid nano-fluid [128].

3.2. ZrO_2 as Material Support for Non-Conventional Storage Energy Systems

Scientific development has led to the emergence of innovative applications in the field of electrical energy devices, which have become essential in everyday life [173–175]. This development has contributed to a significant increase in global electricity consumption, which has amplified energy demand [176–178].

A crucial factor is the efficient storage of energy, given the risk of losses in the case of using inappropriate devices. Supercapacitors offer a sustainable solution, outperforming traditional energy storage devices such as batteries and capacitors. Among the advantages of supercapacitors are their high energy storage capacity, low cost, longer lifetime, shorter charging times, safety, and low environmental impact [173,179]. Supercapacitors are classified into electric double-layer capacitors and pseudocapacitors, the latter having a higher specific capacity and energy densities. The electrode material is very important for the performance of the pseudocapacitor; typically, it is based on nano-oxides of metals such as MnO, RuO_2, TiO_2, SnO_2, ZrO_2, Fe_2O_3, V_2O_5, etc. [180,181]. Nanostructures lead to remarkable physical and chemical properties as nano-ZrO_2 is an excellent optical, thermal, mechanical, and electrical material [182].

Some examples of methods of preparation and characteristics of ZrO_2 NPs used for energy storage applications over the last 10 years are presented in Table 2.

The literature indicates that the hydrothermal fabrication of nano-ZrO_2 and/or nano-Ag doped ZrO_2, which presents a porous surface and high conductivity, leads to better electrochemistry in supercapacitor applications [191].

Fast energy storage capacitors are a current requirement in the field of pulsed power and power electronics technologies, which is the reason why the design of advanced materials and the application of nanotechnologies is in continuous development. In this context, lead-free ceramics have been developed with regard to dielectrics that have a fast charge/discharge rate and long lifetime. An example is $(1-x)(0.6SrTiO_3\text{-}0.4Na_{0.5}Bi_{0.5}TiO_3)\text{-}xZrO_2$ (STNBT-xZr), in which the addition of ZrO_2 synthesized hydrothermally led to a decrease in particle size and an improvement in fracture resistance [124].

Pure ZrO_2 electrodes have high electrical resistance, which restricts their effectiveness as electrode materials in supercapacitors. ZrS_2 materials have been explored as potential electrode materials in Li-ion batteries [192]. Figure 10 shows the stratified arrangement of ZrS_2 and the electrochemical process mechanism in a lithium-ion battery.

Manzoor et al. [193] synthesized a ZrO_2/CdS nanohybrid, which demonstrated an excellent electrochemical response for pseudo-supercapacitor devices. For instance, a high specific capacitance (Cs) of 1391 F/g, specific energy of 48.27 Wh/kg, specific power of 0.0014 Kw/kg at a current density of 2.5 A/g, and excellent stability at 2000 cycles were achieved for ZrO_2/CdS synthesized material using the galvanostatic charge discharge (GCD) (Figure 11). The enhanced electrochemical performance of the zirconia-based supercapacitor electrode materials was attributed to their high conductivity, rapid electron transfer, and large specific surface area.

Table 2. Significant examples of publications regarding the preparation method and characterization of ZrO_2 with potential applications in energy storage over the past 10 years.

No.	Method	Characteristics	Year	Ref.
1.	Relaxor ferroelectric ceramic based on (0.6-x)$Ba_{0.55}Sr_{0.45}TiO_3$-0.4$Bi_{0.5}Na_{0.5}TiO_3$-x$SrZrO_3$ ((0.6-x)BST-0.4BNT-xSZ) is prepared using the tape casting method	Excellent energy density (Wrec ≈ 10.0 J cm^{-3}) and high energy storage efficiency (η ≈ 91%)	2024	[151]
2.	ZrO_2 nanopowder by microwave-assisted hydrothermal synthesis	NPs as nanospheres, nano squares, and some irregularly shaped nanostructures with an average particle size of 6.7 ± 1.9 nm (as-synthesized) and 45.7 ± 9.9 nm (calcined)	2023	[116]
3.	$Pb_{0.88}La_{0.12}ZrO_3$ (PLZ) antiferroelectric films with ZrO_2 as inserting layer by sol-gel method	PLZ film thickness: 355 nm, with ZrO_2 addition: 385 nm, with thickness of sandwiched ZrO_2 layer: 30 nm		[183]
4.	Ag incorporated ZrO_2 nanomaterials by hydrothermal method	ZrO_2 NPs average size of 20–25 nm and the Ag NPs of 15–20 nm	2022	[173]
5.	UiO-66 (Zr-MOF) obtained by thermal conversion. ZrO_2/C composites obtained at 600, 800, and 1000 °C denoted as Z-600, Z-800, and Z1000, respectively	Uniformly distributed ZrO_2 NPs within a porous carbon environment, with an average size of 200 nm	2021	[184]
6.	ZrO_2-polymer nanocomposite porous membranes prepared by the one-step phase inversion method	Surface area for Ni–ZrO_2–rGO is 185.461 m^2 g^{-1}, while for Co–ZrO_2–rGO it is 99.506 m^2 g^{-1}	2020	[185]
7.	The core-shell structured BT@ZrO_2 nanofibers were synthesized through coaxial electrospinning method	$BaTiO_3$@ZrO_2 nanofibers for energy storage device. The outer layer is about 30 nm and the inner rod is about 400 nm in thickness	2019	[186]
8.	STNBT and ZrO_2 powders synthesized by solid-state reaction method and microwave hydrothermal method for 0.6$SrTiO_3$-0.4$Na_{0.5}Bi_{0.5}TiO_3$-xZrO_2 ceramics (STNBT-xZr)	Average grain size 1.6 mm related to the addition of ZrO_2 powders	2018	[124]
9.	~7.1 nm $Hf_{0.5}Zr_{0.5}O_2$ thin films deposited at 215 °C via a thermal atomic layer deposition (ALD) process on a TiN bottom electrode	Energy storage density of ~55 J cm^{-3} with an efficiency of ~57%	2017	[187]
10.	ZrO_2 and reduced graphene oxide (r-GO) composite was synthesized by chemical methods	ZrO_2-rGO nanocomposite exhibited a high surface area of 390 m^2 g^{-1}	2016	[188]
11.	Graphene/ZrO_2 composite aerogels prepared by sol-gel method	The average particle size of the ZrO_2 is less than 10 nm and the specific surface area is 380–490 m^2 g^{-1}	2015	[189]
12.	ZrO_2 nanorods through a hydrothermal process	Average particle size of ZrO_2 ~ 20 nm	2014	[190]

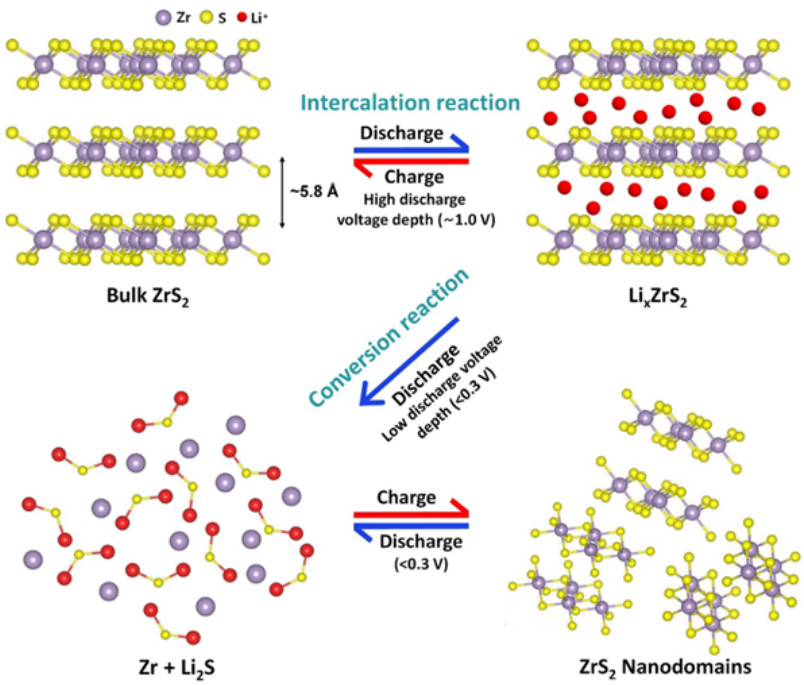

Figure 10. The stratified arrangement of ZrS_2 and the electrochemical process mechanism in a lithium-ion battery. Reprinted with permission from [192].

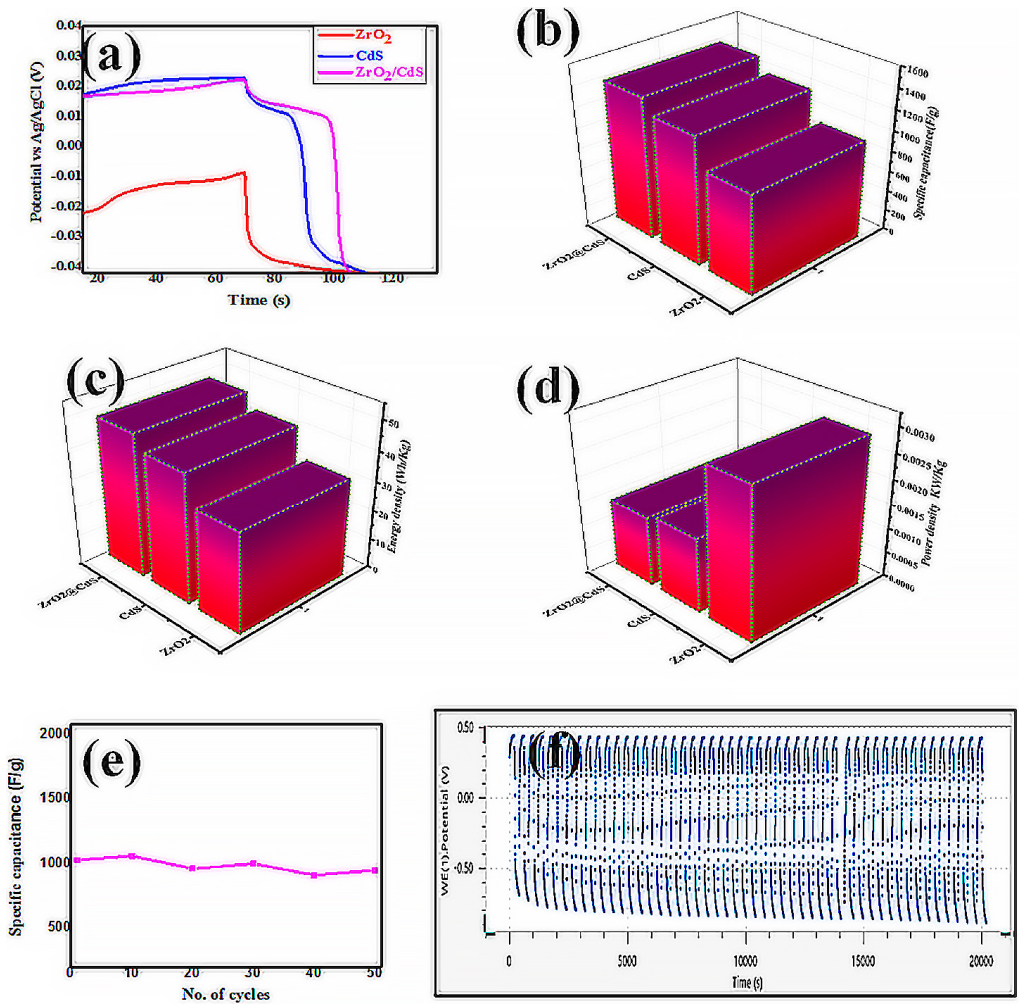

Figure 11. (**a**) GCD, (**b**) Cs, (**c**) specific energy, and (**d**) specific power of ZrO_2, CdS, and ZrO_2/CdS, (**e**) no. of cycles vs. Csp, (**f**) stability cycles. Reprinted with permission from [193].

In another paper, $ZnFe_2O_4$-ZrO_2 nanocomposite was prepared by the hydrothermal synthesis method and demonstrated excellent charge storage and electrocatalytic capabilities, suggesting its use as a supercapacitor material [194]. Thus, a high current density of 104.74 mA/cm^2 and an electrochemical surface area (ECSA) of 46.36 m^2/g, with an onset potential of −0.51 V, were registered for the $ZnFe_2O_4$-ZrO_2 catalyst when Pt was electrochemically deposited on its surface and used for the methanol oxidation reaction (MOR). After 150 cycles, the MOR current increased to 107.2 mA/cm^2 and retained 102.34% of its initial value. The electrocatalytic activity of prepared electrode for MOR was evaluated by cyclic voltammograms (CV), CA, and linear sweep voltammetry (LSV) in 0.5 M KOH with 1 M methanol (Figure 12).

The increased resistivity of ZrO_2 provides oxidation stability, thus being compatible with various electrical and electronic applications with excellent mechanical and chemical properties. Since it presents a wide semiconductor band that extends around 5 eV, it is often preferable to dope it with materials with high optical and electrical properties, such as lanthanides [129,195,196]. The choice of ZrO_2 as an electrode material is also given by the complexity of other materials in the process of obtaining, designing, and testing. Excellent results were obtained for nano ZrO_2/carbon black as an electrode material [197]. Energy storage performance was achieved even after 5000 charge/discharge cycles. Also, the TiO_2/ZrO_2 nanofibers, obtained by electrospinning and the hydrothermal process, had a high specific capacity and good electrochemical response [198]. The production and storage of energy represent a sustainable approach in the context of the circular economy, but a

new challenge is also presented by the capture of incidental sunlight and its transformation into electricity.

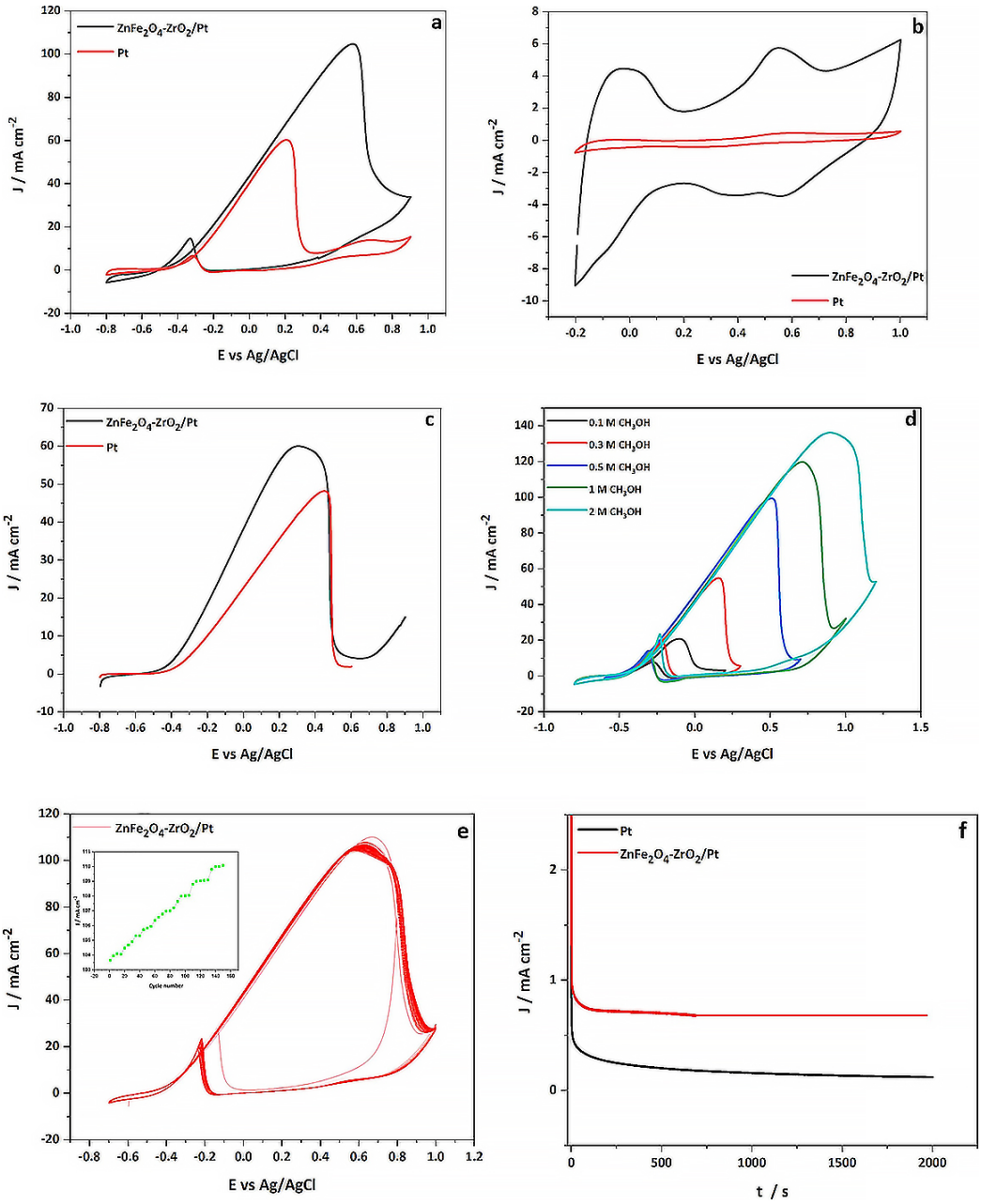

Figure 12. (**a**) CV plots of $ZnFe_2O_4$-ZrO_2/Pt and Pt in 0.5 M KOH with 1 M methanol electrolytes, (**b**) CV plots in 0.5 M KOH, (**c**) LSV curves, (**d**) CV plots in different methanol concentration, (**e**) 150th cycle of new electrolyte at a scan rate of 50 mV/s, (**f**) CA curves of $ZnFe_2O_4$-ZrO_2/Pt and Pt electrodes in 0.5 M KOH, with 1 M methanol at 0.5 V (0–2000 s). Reprinted with permission from [194].

In recent years, the trend has been to develop photovoltaic devices to replace fossil fuels, thus meeting energy requirements [129]. The use of ZrO_2 as an interface material between the transport layer and the absorber is an emerging approach used to passivate defects at the interface. To increase the electrochemical performance, nanoscale ZrO_2 is used with other composites or alloys, and lanthanide oxides such as Sm/Eu/Tm. The bandgap energies are thus reduced from 4.04 to 3.57 eV, and the crystallite sizes decrease from 67.92 to 45.23 nm, leading to the improvement of the optoelectronic properties.

Nanocrystalline ZrO_2, ZnO, and SiO_2-coated ZrO_2 core-shell structures were synthesized using both co-precipitation and seeded polymerization techniques, showing promise as optical-electronic devices [199].

Abhisek et al. [200] demonstrated through FESEM analysis a morphological transition from nanoclusters of small ZrO_2 particles (Figure 13a,b) and stacked NiO flakes (Figure 13c,d) to self-assembled ZNC nanotorous structures (Figure 13e–g). It can be observed that each NiO flake consists of tiny particles that have self-organized into nanoclusters, creating a central void typical of a nanotorous-like structure. The particles within the nanoporous flakes show a high degree of order and uniform decoration, with no evidence of agglomeration. This organization resulted in the formation of vacancies, which could enhance the electrochemical performance of the composite. The average particle size was found to be 49.54 nm, with a mean pore diameter of 20.15 nm.

Monoclinic ZrO_2 shows abundant hydroxyl functional groups on the surface, as shown by the IR vibration spectra, that determine an intense electrocatalytic activity of the nanoparticles. This property has been used in the production of the electrocatalyst for the electrochemical generation of hydrogen, with hydrogen release increasing as the content of the monoclinic phase rises, compared to the tetragonal phase. Hydrothermal synthesis at acidic pH was also selected for the production of monoclinic nano-ZrO_2 [201].

Antiferroelectric materials also belong to the category of dielectric capacitors, with efficient energy storage, which have the advantage of obtaining high photogenerated voltages that cannot be achieved by green polymers or only by metal oxides [202,203]. These high-power materials show almost zero remanent polarization and performance in the phase transition process [204,205]. An example is the $Pb_{0.88}La_{0.12}ZrO_3$ antiferroelectric films, where a ZrO_2 insertion layer was deposited on $LaNiO_3/SiO_2/Si$ substrates using the sol-gel method [183]. Tests indicated that the insertion of the ZrO_2 layer leads to superior fracture toughness and energy storage properties.

Al_2O_3/ZrO_2 and $Al_2O_3/ZrO_2(Y_2O_3)$ eutectic ceramics show excellent mechanical properties at high temperatures [206]. ZrO_2 acts as a stabilizer, and the added amount can provide control over the phase and the microstructure. ZrO_2 can also be obtained in the form of fibers with superior microstructure and mechanical properties. The growth speed of the fibers also leads to an increase in breaking hardness and fracture toughness [206,207].

To investigate the heterogeneous charge transfer behavior of the analyte and the electrode–electrolyte interface, electrochemical impedance spectroscopy (EIS) is performed. The corrosion behavior of bare zirconia nanotubes (ZNTs) and Chitosan PEDOT (ChP)-ZNTs hybrid nanocomposite was studied in electrochemical studies [208]. EIS was conducted in freshly prepared Hanks' solution, and the results were presented as a Nyquist plot, as shown in Figure 14. Data showed that ChP-ZNTs exhibit superior corrosion inhibition.

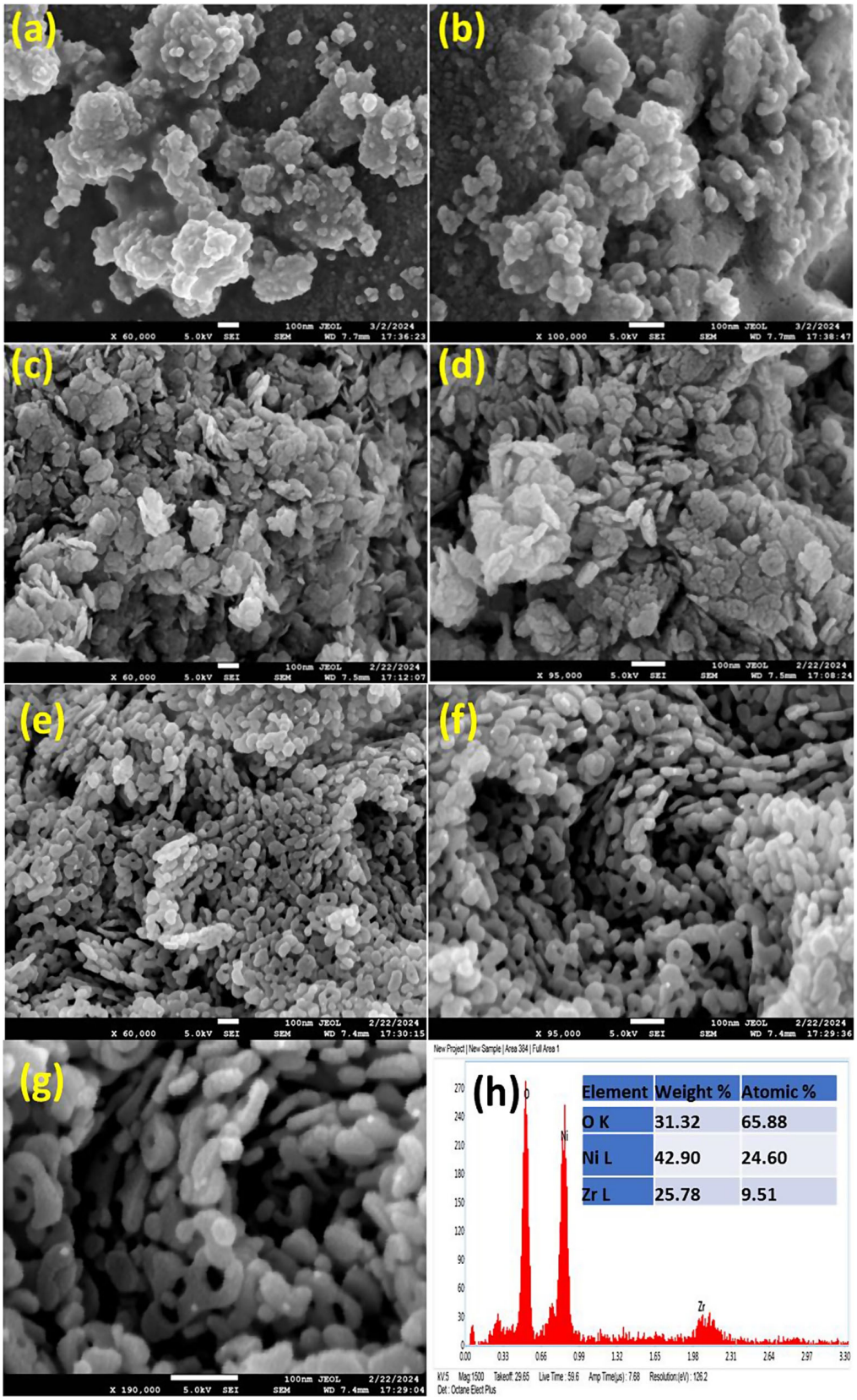

Figure 13. (**a**–**h**) FESEM micrograph of (**a**,**b**) pure ZrO_2, (**c**,**d**) pure NiO, (**e**–**g**) ZNC, (**h**) EDAX and percentage composition of each element in the ZrO_2-NiO composite (ZNC). Reprinted with permission from [200].

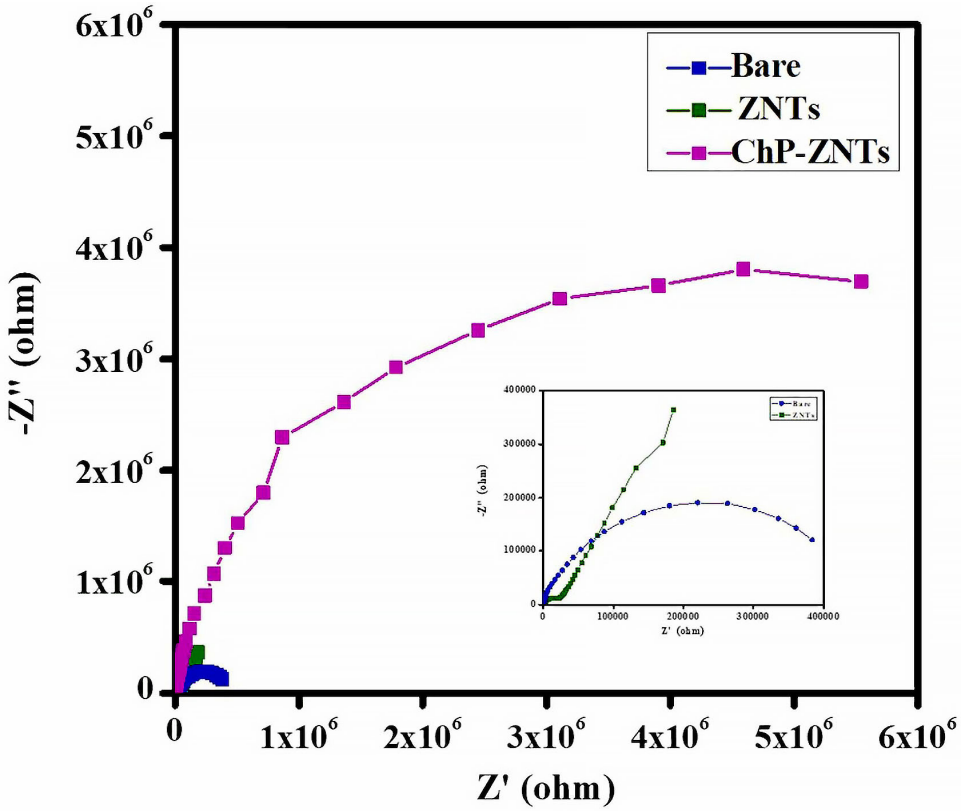

Figure 14. Electrochemical impedance spectroscopic studies' Nyquist plot of bare ZNTs and ChP-ZNTs. Reprinted with permission from [208].

3.3. Other Applications

3.3.1. Biomedical Applications

The continuous development of antibiotics and antifungal pharmaceutical products as a result of problems related to antibiotic resistance has led to the need to identify alternatives to reduce infections, with bionanotechnology emerging as a frequently used alternative. Today, metallic nanomaterials with antibacterial and antifungal properties are used. For example, Ag NPs [209] and nano-ZrO_2 synthesized by biosynthesis from botanical and microbial sources represent environmentally friendly synthesis alternatives [35]. The biocompatibility of nano-ZrO_2 is given by its size and large specific surface, and the positive charge of the nanoparticles develops electrostatic interactions with the bacteria, which are mostly made up of negatively charged proteins, thus leading to biosorption and bioaccumulation on the cell walls [35]. The literature indicates excellent results in the antibacterial activity of nano-ZrO_2 obtained from green synthesis on gram-negative and gram-positive bacteria.

3.3.2. Environmental Protection

Zirconia composites are gaining significant attention in environmental applications due to their exceptional properties, such as high mechanical strength, excellent chemical stability, corrosion resistance, and biocompatibility. Table 3 shows some key environmental applications of nano-zirconia composites synthesized by green synthesis as excellent adsorbents.

The presence of emerging pollutants, such as antibiotics, contributes today to the massive pollution of water sources, especially through discharge from hospital and urban treatment plants, and leads to antibiotic resistance in aquatic flora and fauna, subsequently influencing water quality [35]. A risk is also presented by pollutants' non-biodegradable nature and the lack of effective removal methods. Adsorption remains the most viable method up to now to be used for removing emerging pollutants [222–224]. Thus, the

appropriate selection and specificity of nanomaterials chosen for water treatment become very important.

Table 3. ZrO_2 NPs and its composites for environmental applications.

No.	Green Synthesis Method	Results and Application	Ref.
1.	*Sonchus asper* leaves extract was mixed with $ZrOCl_2 \cdot 8H_2O$ (0.1 M) in the ratio of 1:1 (*v*/*v*)	ZO-500 NPs presented an adsorptive capacity for Amoxicillin (AMX) in an aqueous solution of 180.5 mg/g	[210]
2.	Henna extract was mixed with 0.2 M of $ZnSO_4 \cdot 7H_2O$ and 0.2 M of $ZrCl_4$ and microwaved at 175 °C for 15 min, then the ZrO_2/ZnO material was embedded on activated carbon	ZrO_2/ZnO/AC at a pH of 2 with methyl orange (MO) degradation of 80%	[211]
3.	Extract from *Sapindus mukorossi* added to a 0.1 M $ZrOCl_2 \cdot 8H_2O$ in the ratio of 1:1 (*v*/*v*)	ZrO_2 NPs used as adsorbents for Methylene blue (MB) removal at pH 10, 0.3 g adsorbent dosage, initial MB concentration 20 mg/L, 300 min 94% removal efficiency, and adsorptive capacity of 23.26 mg/g	[212]
4.	*Wrightia tinctoria* leaf extract was added drop wise into 10 mL of (0.1 M) aqueous $ZrOCl_2 \cdot 8H_2O$ solution under vigorous stirring at 75 °C for 3–4 h	ZrO_2 NPs used for catalytic degradation of reactive yellow 160 dye, the degradation efficiency of 94.58% after 120 min.	[213]
5.	Bacteria *Pseudomonas aeruginosa*, grown for 96 h, centrifugation at 10,000 rpm for 15 min resulting in cell-free supernatant, which was added to a zirconium oxychloride octahydrate solution (20 mM)	ZrO_2 NPs used as adsorbents for tetracycline, the adsorption capacity of 526.32 mg/g at pH 6,Reusability up to 5 cycles (81.55% after the 5th cycle)	[214]
6.	20 mL of the *Daphne alpine* leaf extract was mixed with 50 mL of ammonium meta-vanadate solution (5 mM) and 20 mL with 50 mL of zircon (IV) chloride solution (5 mM), then the 2 gels were mixed together	V_2O_5/ZrO_2 nanomaterial. The degradation efficiencies of V_2O_5/ZrO_2 against methyl orange (76.9%) and picloram (86%) for 75 min	[215]
7.	Precipitation between extract from roots of *Euclea natalensis* added to a zyrconil chloride solution	ZrO_2 white nanopowder is used for tetracycline adsorption, with an adsorption capacity of 30.45 mg/g	[216]
8.	20 mL of *Ficus benghalensis* leaf extract was added dropwise into 20 mL of (0.1 M) aqueous $ZrOCl_2 \cdot 8H_2O$ solution	ZrO_2 NPs used for catalytic degradation of methyl orange (MO) at pH degradation efficiency of 69.23% after 240 min, and MB removal of 91.22% after 240 min	[217]
9.	*Lagerstroemia speciosa* leaf extract added to zirconium nitrate 0.2 N solution, stirred continuously at 90 °C for 3 h	ZrO_2 NPs used for MO degradation of 94.58% after irradiating under the sunlight for 290 min	[218]
10.	*Leucas aspera* leaf extract with an aqueous Zirconyl nitrate mixture was subsequently added to Samarium nitrate solution	ZrO_2: Sm^{3+} nanomaterial Sm^{3+}/ZrO^{2+} = 3–11 mol.%), High sunlight-driven degradation of 83.8% for acid green dye after 90 min.	[219]
11.	ZrO_2: Mg (0.1 mol%) NPs were synthesized by low-temperature phyto combustion route using *Aloe Vera* gel extract	ZrO_2–Mg (2 mol.%) gave the highestRhodamine B degradation efficiency (93%)	[220]
12.	Precipitation of zirconia NPs using *Aloe Vera* extract with a solution of $ZrOCl_2 \cdot 8H_2O$ (10 mM). The NPs were embedded in chitosan beads (CNZr)	Nearly 99% F–ions were adsorbed byCNZr, chemisorption capacity of 96.58 mg/g	[221]

There are reports of the removal of antibiotics [210,214,216], dyes [210,212,213,215,217–220], and fluor [221] in the presence of nano-zirconia/zirconia compounds synthesized by green methods. For instance, the tetracycline elimination process using nano-ZrO_2 obtained by biosynthesis was accomplished at an adsorption capacity from 30.45 mg/g to 526.32 mg/g, and at up to five cycles of reuse [215,216]. It is known that the photosynthesis process slows down or even stops in water where paints are present, as a result of blocking the penetration of sunlight into the depth of the water, and implicitly affecting aquatic life.

The degradation of these emerging pollutants is difficult as they are very stable, so adsorption and photocatalysis remain alternatives [35,225,226]. Nano-ZrO_2 from green synthesis had 94% efficiency for the removal of methylene blue (MB), with a low adsorption capacity of about 23.25 mg/g and the possibility of reuse for three consecutive cycles [212].

The dyes were tested for the possibility of degradation using Zr-based composites, such as zirconium-manganese nanocomposite (Zr/Mn) and zirconium iron (Zr/Fe) as catalysts for the degradation of alizarin red S (AS). The removal efficiency was 99% in the presence of UV light and 95% in the presence of sunlight [133]. The degradation efficiency using nano-ZrO_2 of 99% was also obtained for methyl orange, but also for rhodamine B using mesoporous ceramics of the ZrO_2–CeO_2–TiO_2 type in visible light, and oxidation for alcohol using MnO_2/TiO_2-ZrO_2 [133]. The plant extract can significantly contribute to the formation of nano-ZrO_2 with a reduced size and narrower bandgap energy (3.78 eV).

ZrO_2@SiO_2 core–shell nanostructures were successfully synthesized by Padovini et al. [227] using both the hydrothermal and Stöber methods. These nanostructures demonstrated photocatalytic activity toward rhodamine B (RhB) in pollutant solutions. This enhanced performance is attributed to the Zr-O-Si interfacial layer, which narrows the energy gap (2.31 eV) required for electron-hole pair generation.

In water, fluoride ions are an aggressive pollutant with an impact on bones; nano-ZrO_2 from Aloe Vera extract showed an adsorption efficiency of about 99% [221,228]. The studies in the literature indicate results that lead to the continuation of research regarding the use of nano-ZrO_2 obtained from plant extracts for the removal of various pollutants from water. For example, nano-ZrO_2 could be obtained at a particle size of about 21 nm using lemon juice or tuber powder [229,230].

Another environmental application is nano-ZrO_2 obtained by the hydrothermal method (simple or doped with Ag), and which is used as a catalyst in the oxidation of diesel soot and, implicitly, for suspended particles (PM) [117].

An important application in the field of environmental protection is the study of the corrosion of steels that are part of metal structures, cutting equipment, gas sensors, refractory materials, etc. Good results of inhibiting the corrosion process on a mild steel were obtained using polymer composites of PVDF/ZrO_2. The role of ZrO_2 doping with stabilizers is to obtain high strength and fracture toughness [231]. Nano-ZrO_2 is also used in composites with aluminum to increase the coefficient of friction and resistance to wear, traction, impact, microhardness, and fracture toughness [232].

In metallurgy, the manufacture of sensors for the detection of unwanted microelements in molten steel is in continuous development. The ZrO_2 (MgO) electrolyte has been studied in this respect, presenting an effect on the measurement of the low oxygen potential, together with 6MgO–2Y_2O_3–ZrO_2, obtained by sintering without pressure [233].

The photocatalytic role of nanomaterials is well known for the degradation and oxidation of emerging organic pollutants. A C_3N_4/ZrO nanostructure containing graphitic carbon nitride (C_3N_4), and zirconium oxide (ZrO_2) obtained by direct thermal pyrolysis, were tested in the process of the photocatalytic degradation of a mixture of dyes, Rh B + crystal violet (CV), and the reaction of methanol oxidation [233]. An efficiency of 97% was obtained in the degradation of the dye mixture, and for methanol the oxidation activity of the nanostructure was exceptionally high, at a current of 138.25 mA/cm^2 for 2 M methanol [234].

4. Conclusions and Perspectives

This review presents the most important aspects related to the synthesis methods and future applications in the field of energy conservation and storage. ZrO_2 nanoparticles represent a material of the future in the context of preserving natural resources and identifying sustainable solutions for energy conservation and storage. It is a non-toxic material for environment with a wide band gap and short-wavelength luminescence properties.

The applications for which ZrO_2 is a basic material are essential today in the development of society towards a clean environment. Nano-ZrO_2 presents high-temperature stability and corrosion resistance, and these properties give it versatility for a multitude of applications from refractory ones to medical products, pigments, electronics, coatings, and ceramics. However, an important aspect is represented by the synthesis methods by which nano-ZrO_2 can be obtained. Although compared to other oxide materials specific to the same field, research on the synthesis and applications for nano-ZrO_2 is limited, a trend can be observed regarding the interest in applications regarding energy conversion compared to storage. Also, in terms of research on the synthesis of nano-ZrO_2, the most used methods are those specific to the bottom-up approach, the most applied being sol-gel, followed by precipitation and hydrothermal synthesis. There is an interest, especially in the last five years, for green synthesis, but this is in an early stage.

While zirconium-based materials offer excellent properties, their high cost and complex processing requirements (e.g., high-temperature production, specialized alloys) can

limit their widespread adoption. The development of zirconia-based materials in term of high energy and power density to achieve the maximum goal is still a key challenge.

Advances in processing technologies and the recycling of Zr alloys could make them more economically viable. Continued research into new alloys, processing techniques, and applications in emerging fields like hydrogen storage and quantum computing will expand the range of potential uses for zirconium in the future. Green synthesized ZrO_2 NPs and their corresponding nanocomposites are anticipated to yield promising outcomes across a wide range of applications. Further research is needed to optimize the properties of zirconia composites for specific environmental applications, such as improving adsorption capacity and selectivity, and the integration of zirconia with other materials for enhanced performance. In addition, the potential ecotoxicity of nano-zirconia remains a subject that must be addressed further.

Author Contributions: Conceptualization, E.M. and M.P.; methodology, E.M.; validation, R.Ș. and C.P.; formal analysis, M.R.; resources, R.R.P.; writing—original draft preparation, E.M. and M.P.; writing—review and editing, A.-A.Ș. and M.R.; visualization, E.M., A.-A.Ș. and M.R.; supervision, R.R.P., R.Ș. and C.P. All authors have read and agreed to the published version of the manuscript.

Funding: This research received no external funding.

Acknowledgments: E. Matei and A.-A. Șăulean acknowledge the grant from the National Program for Research of the National Association of Technical Universities—GNAC ARUT 2023.

Conflicts of Interest: The authors declare no conflicts of interest.

References

1. Zhang, H.; Lu, Y.; Han, W.; Zhu, J.; Zhang, Y.; Huang, W. Solar energy conversion and utilization: Towards the emerging photo-electrochemical devices based on perovskite photovoltaics. *Chem. Eng. J.* **2020**, *393*, 124766. [CrossRef]
2. Ritchie, H.; Roser, M. Renewable Energy. 2020. Available online: https://OurWorldInData.org (accessed on 3 September 2024).
3. Robinson, J.; Kumari, N.; Srivastava, V.K.; Taskaeva, N.; Mohan, C. Sustainable and environmental friendly energy materials. *Mater. Today Proc.* **2022**, *69*, 494–498. [CrossRef]
4. Kumar, N.; Shahzeb Hasan, S.; Srivastava, K.; Akhtar, R.; Kumar Yadav, R.; Choubey, V.K. Lean manufacturing techniques and its implementation: A review. *Mater. Today Proc.* **2022**, *64*, 1188–1192. [CrossRef]
5. Nikitina, A.A.; Lavrentev, F.V.; Yurova, V.Y.; Piarnits, D.Y.; Volkova, O.O.; Skorb, E.V.; Shchukin, D.G. Layered nanomaterials for renewable energy generation and storage. *Mater. Adv.* **2024**, *5*, 394–408. [CrossRef]
6. Minakshi, M.; Mujeeb, A.; Whale, J.; Evans, R.; Aughterson, R.; Shinde, P.A.; Ariga, K.; Shrestha, L.K. Synthesis of Porous Carbon Honeycomb Structures Derived from Hemp for Hybrid Supercapacitors with Improved Electrochemistry. *ChemPlusChem* **2024**, *n/a*, e202400408. [CrossRef] [PubMed]
7. Minakshi, M.; Samayamanthry, A.; Whale, J.; Aughterson, R.; Shinde, P.A.; Ariga, K.; Kumar Shrestha, L. Phosphorous—Containing Activated Carbon Derived From Natural Honeydew Peel Powers Aqueous Supercapacitors. *Chem.—Asian J.* **2024**, *19*, e202400622. [CrossRef]
8. Yan, F.; Qian, J.; Wang, S.; Zhai, J. Progress and outlook on lead-free ceramics for energy storage applications. *Nano Energy* **2024**, *123*, 109394. [CrossRef]
9. de Araújo-Júnior, E.N.S.; Bergamo, E.T.P.; Bastos, T.M.C.; Benalcázar Jalkh, E.B.; Lopes, A.C.O.; Monteiro, K.N.; Cesar, P.F.; Tognolo, F.C.; Migliati, R.; Tanaka, R.; et al. Ultra-translucent zirconia processing and aging effect on microstructural, optical, and mechanical properties. *Dent. Mater.* **2022**, *38*, 587–600. [CrossRef]
10. Fujii, S.; Shimazaki, K.; Kuwabara, A. Empirical interatomic potentials for ZrO_2 and YSZ polymorphs: Application to a tetragonal ZrO_2 grain boundary. *Acta Mater.* **2024**, *262*, 119460. [CrossRef]
11. Mohan, P.; Yuan, B.; Patterson, T.; Desai, V.H.; Sohn, Y.H. Degradation of Yttria-Stabilized Zirconia Thermal Barrier Coatings by Vanadium Pentoxide, Phosphorous Pentoxide, and Sodium Sulfate. *J. Am. Ceram. Soc.* **2007**, *90*, 3601–3607. [CrossRef]
12. Lovisa, L.X.; Gomes, E.; Gracia, L.; Santiago, A.; Li, M.; Andres, J.; Longo, E.; Bomio, M.; Motta, F. Integrated experimental and theoretical study on the phase transition and photoluminescent properties of ZrO_2:xTb^{3+} (x = 1, 2, 4 and 8 mol %). *Mater. Res. Bull.* **2021**, *145*, 111532. [CrossRef]
13. Kuo, C.-W.; Lee, K.-C.; Yen, F.-L.; Shen, Y.-H.; Lee, H.-E.; Wen, S.-B.; Wang, M.-C.; Stack, M.M. Growth kinetics of tetragonal and monoclinic ZrO_2 crystallites in 3mol% yttria partially stabilized ZrO_2 (3Y-PSZ) precursor powder. *J. Alloys Compd.* **2014**, *592*, 288–295. [CrossRef]
14. Qi, B.; Liang, S.; Li, Y.; Zhou, C.; Yu, H.; Li, J. ZrO_2 Matrix Toughened Ceramic Material-Strength and Toughness. *Adv. Eng. Mater.* **2022**, *24*, 2101278. [CrossRef]

15. Foo, Y.T.; Abdullah, A.Z.; Amini Horri, B.; Salamatinia, B. Optimised Co-Precipitation synthesis condition for oxalate-derived zirconia nanoparticles. *Ceram. Int.* **2019**, *45*, 22930–22939. [CrossRef]
16. Chintaparty, R.; Palagiri, B.; Nagireddy, R.R.; Reddy, V.S.R.I. Effect of phase transformation on optical and dielectric properties of zirconium oxide nanoparticles. *Phase Transit.* **2015**, *88*, 929–938. [CrossRef]
17. Rabiey, M.; Jochum, N.; Kuster, F. High performance grinding of zirconium oxide (ZrO_2) using hybrid bond diamond tools. *CIRP Ann.* **2013**, *62*, 343–346. [CrossRef]
18. Lakhloufi, S.; Labjar, N.; Labjar, H.; Serghini- Idrissi, M.; El Hajjaji, S. Electrochemical behavior and surface stability of dental zirconia ceramics in acidic environments. *J. Mech. Behav. Biomed. Mater.* **2024**, *150*, 106288. [CrossRef]
19. Tao, Z.; Yin, H.; Lv, Y.; Guo, H.; Chen, J.S.; Ye, X.; Xian, H.; Sun, S.; Li, T. Crystalline modulation of zirconia for efficient nitrate reduction to ammonia under ambient conditions. *Chem. Commun.* **2024**, *60*, 5554–5557. [CrossRef]
20. Kim, D.; Yun, H.; Kim, J.; Lee, C.W.; Hwang, Y.J. Enhanced C–C coupling of Cu-based catalysts via zirconia-driven carbonate interaction for electrochemical CO_2 reduction reaction. *J. Mater. Chem. A* **2024**, *12*, 23780–23788. [CrossRef]
21. Lang, J.; Ren, K.; Wang, Y. CaO–MgO–Al_2O_3–SiO_2 Corrosion Resistance of Multi-Rare-Earth-Oxide-Doped Zirconia Thermal Barrier Coating. *Ceram. Int.* **2024**, *50*, 30373–30380. [CrossRef]
22. Yang, G.; Han, C.; Chen, Y.; Guo, F.; Lu, J.; Zhou, M.; Luo, L.; Zhao, X. Interfacial Stability between High-Entropy $(La_{0.2}Yb_{0.2}Sm_{0.2}Eu_{0.2}Gd_{0.2})_2Zr_2O_7$ and Yttria-Stabilized Zirconia for Advanced Thermal Barrier Coating Applications. *Coatings* **2024**, *14*, 269. [CrossRef]
23. Zhang, Q.; Kong, J.; Ye, S.; Lu, K.; Hao, Y.; Wu, W.; Xiong, G.; Wang, Y.; Xu, S.; Deng, W. Highly efficiency up and down -conversion photoluminescence in Er/Tm/Yb co-doped lutecia-stabilized zirconia single crystals. *J. Alloys Compd.* **2024**, *1008*, 176551. [CrossRef]
24. Kilic, U.; Traouli, Y.; Hilfiker, M.; Bryant, K.; Schoeche, S.; Feder, R.; Argyropoulos, C.; Schubert, E.; Schubert, M. Nanocolumnar Metamaterial Platforms: Scaling Rules for Structural Parameters Revealed from Optical Anisotropy. *Adv. Opt. Mater.* **2024**, *12*, 2302767. [CrossRef]
25. Singh, P.V.; Reche, A.; Paul, P.; Agarwal, S. Zirconia Facts and Perspectives for Biomaterials in Dental Implantology. *Cureus* **2023**, *15*, e46828. [CrossRef]
26. Khan, F.; Hossain, N.; Mim, J.J.; Rahman, S.M.M.; Iqbal, M.J.; Billah, M.; Chowdhury, M.A. Advances of composite materials in automobile applications—A review. *J. Eng. Res.* 2024; *in press*. [CrossRef]
27. Musadiq Anis, S.; Habibullah Hashemi, S.; Nasri, A.; Sajjadi, M.; Eslamipanah, M.; Jaleh, B. Decorated ZrO_2 by Au nanoparticles as a potential nanocatalyst for the reduction of organic dyes in water. *Inorg. Chem. Commun.* **2022**, *141*, 109489. [CrossRef]
28. Ashrafi, P.; Nematollahi, D.; Shabanloo, A.; Ansari, A.; Eslamipanah, M.; Jaleh, B. A detailed electrochemical study of anti-malaria drug hydroxychloroquine: Application of a highly porous 3D multi-metal oxide carbon felt/β-PbO_2-ZrO_2_MoO_x electrode for its electrocatalytic degradation. *Electrochim. Acta* **2023**, *458*, 142555. [CrossRef]
29. Geetha, M.; Vashisht, N.B.; Thanvir, S.; Roslan, N.C.; Mohamedzain, T.H.; Alfarwati, S.; Al-Lohedan, H.; Rajabathar, J.R.; Zaidi, S.A.; Sadasivuni, K.K. Multi-functional nanoscale ZrO_2 catalysts for sustainable water treatment. *Mater. Chem. Phys.* **2024**, *316*, 129096. [CrossRef]
30. Gurushantha, K.; Renuka, L.; Anantharaju, K.S.; Vidya, Y.S.; Nagaswarupa, H.P.; Prashantha, S.C.; Nagabhushana, H. Photocatalytic and Photoluminescence studies of ZrO_2/ZnO nanocomposite for LED and Waste water treatment applications. *Mater. Today Proc.* **2017**, *4*, 11747–11755. [CrossRef]
31. Ghiță, A.-N.; Slobozeanu, A.E.; Licu, L.; Ciobota, C.F.; Sobetkii, A.; Vasile, B.S.; Miculescu, F.; Piticescu, R.R. Hydrothermal synthesis of zirconia doped with naturally mixed rare earths oxides and their electrochemical properties for possible applications in solid oxide fuel cells. *Manuf. Rev.* **2024**, *11*, 1. [CrossRef]
32. Da, Y.; Xiao, Y.; Zhong, Z.; Pan, Z.; Jiao, Z. Predictions on conductivity and mechanical property evolutions of yttria-stabilized zirconia in solid oxide fuel cells based on phase-field modeling of cubic-tetragonal phase transformation. *J. Eur. Ceram. Soc.* **2022**, *42*, 3489–3499. [CrossRef]
33. Akhkozov, L.; Danilenko, I.; Podhurska, V.; Shylo, A.; Vasyliv, B.; Ostash, O.; Lyubchyk, A. Zirconia-based materials in alternative energy devices—A strategy for improving material properties by optimizing the characteristics of initial powders. *Int. J. Hydrogen Energy* **2022**, *47*, 41359–41371. [CrossRef]
34. Bortot Coelho, F.E.; Magnacca, G.; Boffa, V.; Candelario, V.M.; Luiten-Olieman, M.; Zhang, W. From ultra to nanofiltration: A review on the fabrication of ZrO_2 membranes. *Ceram. Int.* **2023**, *49*, 8683–8708. [CrossRef]
35. Tran, T.V.; Nguyen, D.T.C.; Kumar, P.S.; Din, A.T.M.; Jalil, A.A.; Vo, D.-V.N. Green synthesis of ZrO_2 nanoparticles and nanocomposites for biomedical and environmental applications: A review. *Environ. Chem. Lett.* **2022**, *20*, 1309–1331. [CrossRef] [PubMed]
36. Rana, A.; Yadav, K.; Jagadevan, S. A comprehensive review on green synthesis of nature-inspired metal nanoparticles: Mechanism, application and toxicity. *J. Clean. Prod.* **2020**, *272*, 122880. [CrossRef]
37. Nguyen, D.T.C.; Nguyen, T.T.; Le, H.T.N.; Nguyen, T.T.T.; Bach, L.G.; Nguyen, T.D.; Vo, D.-V.N.; Van Tran, T. The sunflower plant family for bioenergy, environmental remediation, nanotechnology, medicine, food and agriculture: A review. *Environ. Chem. Lett.* **2021**, *19*, 3701–3726. [CrossRef]
38. Alami, A.H.; Aokal, K.; Zhang, D.; Taieb, A.; Faraj, M.; Alhammadi, A.; Ashraf, J.M.; Soudan, B.; El Hajjar, J.; Irimia-Vladu, M. Low-cost dye-sensitized solar cells with ball-milled tellurium-doped graphene as counter electrodes and a natural sensitizer dye. *Int. J. Energy Res.* **2019**, *43*, 5824–5833. [CrossRef]

39. Mosavari, M.; Khajehhaghverdi, A.; Mehdinavaz Aghdam, R. Nano-ZrO_2: A review on synthesis methodologies. *Inorg. Chem. Commun.* **2023**, *157*, 111293. [CrossRef]
40. Baslayici, S.; Gulen, B.; Bugdayci, M.; Demircivi, P. Facile synthesis of silicon carbide/hydroxyapatite composites through ball-mill for enhancing adsorption of tetracycline. *Int. J. Environ. Anal. Chem.* **2023**, 1–19. [CrossRef]
41. Kanmaz, N.; Bugdayci, M.; Demircivi, P. Exploring photocatalytic tetracycline removal performance under simulated sunlight irradiation: Milling time effect on metallic reduction of MnO/ZrO_2 mixed oxide. *Ceram. Int.* **2024**, *50*, 44598–44608. [CrossRef]
42. Zakeri, M.; Rahimipour, M.; Jamal Abbasi, B. Synthesis of nanostructure tetragonal ZrO_2 by high energy ball milling. *Mater. Technol. Adv. Perform. Mater.* **2013**, *28*, 181–186. [CrossRef]
43. Macan, J.; Brckovic, L.; Gajovic, A. Influence of preparation method and alumina content on crystallization and morphology of porous yttria stabilized zirconia. *J. Eur. Ceram. Soc.* **2017**, *37*, 3137–3149. [CrossRef]
44. Abid, N.; Khan, M.; Shujait, S.; Chaudhary, K.; Ikram, M.; Imran, M.; Haider, J.; Khan, M.; Khan, Q.; Maqbool, M. Synthesis of nanomaterials using various top-down and bottom-up approaches, influencing factors, advantages, and disadvantages: A review. *Adv. Colloid Interface Sci.* **2022**, *300*, 102597. [CrossRef] [PubMed]
45. Garg, R.; Gonuguntla, S.; Sk, S.; Iqbal, M.S.; Dada, A.O.; Pal, U.; Ahmadipour, M. Sputtering thin films: Materials, applications, challenges and future directions. *Adv. Colloid Interface Sci.* **2024**, *330*, 103203. [CrossRef] [PubMed]
46. Kondaiah, P.; Rao, G.M.; Uthanna, S. Preparation of magnetron sputtered ZrO_2 films on Si for gate dielectric application. *J. Phys. Conf. Ser.* **2012**, *390*, 012031. [CrossRef]
47. Verma, M.; Kumar, V.; Katoch, A. Synthesis of ZrO_2 nanoparticles using reactive magnetron sputtering and their structural, morphological and thermal studies. *Mater. Chem. Phys.* **2018**, *212*, 268–273. [CrossRef]
48. Patel, U.; Patel, K.; Chauhan, K.; Chawla, A.; Rawal, S. Investigation of various properties for zirconium oxide films synthesized by sputtering. In Proceedings of the 3rd International Conference on Innovations in Automation and Mechatronics Engineering 2016, ICIAME 2016, Amsterdam, The Netherlands, 5–6 February 2016; pp. 336–343.
49. Balasubramanian, S.; Raghavan, S. Wet Etching of Heat Treated Atomic Layer Chemical Vapor Deposited Zirconium Oxide in HF Based Solutions. *Jpn. J. Appl. Phys.* **2008**, *47*, 4502. [CrossRef]
50. Lowalekar, V.; Raghavan, S. Etching of Zirconium Oxide, Hafnium Oxide, and Hafnium Silicates in Dilute Hydrofluoric Acid Solutions. *J. Mater. Res.* **2004**, *19*, 1149–1156. [CrossRef]
51. Perng, B.-C.; Chen, F.-C.; Tao, H.-J.; Hsu, P.-F.; Hsieh, Y.-H.; Wang, C.-C.; Hsiao, S.-Y. Wet Etchant Composition and Method for Etching HfO2 and ZrO2. U.S. Patent No. 6,969,688, 29 November 2005.
52. Castell, R.; Poirier, T. Laser ablation in the synthesis of zirconium oxide. *Astrophys. Space Sci.* **1997**, *256*, 539–545. [CrossRef]
53. Tan, D.; Lin, G.; Liu, Y.; Teng, Y.; Zhuang, Y.; Zhu, B.; Zhao, Q.; Qiu, J. Synthesis of nanocrystalline cubic zirconia using femtosecond laser ablation. *J. Nanopart. Res.* **2011**, *13*, 1183–1190. [CrossRef]
54. Vrejoiu, I.; Matei, D.; Morar, M.; Epurescu, G.; Ferrari, A.; Balucani, M.; Lamedica, G.; Dinescu, G.; Grigoriu, C.; Dinescu, M. Properties of ZrO_2 thin films prepared by laser ablation. *Mater. Sci. Semicond. Process.* **2002**, *5*, 253–257. [CrossRef]
55. Amendola, V.; Meneghetti, M. Laser ablation synthesis in solution and size manipulation of noble metal nanoparticles. *Phys. Chem. Chem. Phys.* **2009**, *11*, 3805–3821. [CrossRef] [PubMed]
56. Wang, J.; Valenzuela, M.; Salmones, J.; Vázquez, A.; Garcıa-Ruiz, A.; Bokhimi, X. Comparative study of nanocrystalline zirconia prepared by precipitation and sol–gel methods. *Catal. Today* **2001**, *68*, 21–30. [CrossRef]
57. Behbahani, A.; Rowshanzamir, S.; Esmaeilifar, A. Hydrothermal synthesis of zirconia nanoparticles from commercial zirconia. *Procedia Eng.* **2012**, *42*, 908–917. [CrossRef]
58. Shaik, M.; Alam, M.; Adil, S.; Kuniyil, M.; Al-Warthan, A.; Siddiqui, M.; Tahir, M.; Labis, J.; Khan, M. Solvothermal Preparation and Electrochemical Characterization of Cubic ZrO_2 Nanoparticles/Highly Reduced Graphene (HRG) based Nanocomposites. *Materials* **2019**, *12*, 711. [CrossRef]
59. Liu, X.; Pappas, I.; Fitzgerald, M.; Zhu, Y.; Eibling, M.; Pan, L. Solvothermal synthesis and characterization of ZrO_2 nanostructures using zirconium precursor. *Mater. Lett.* **2010**, *64*, 1591–1594. [CrossRef]
60. Stolzenburg, P.; Freytag, A.; Bigall, N.; Garnweitner, G. Fractal growth of ZrO_2 nanoparticles induced by synthesis conditions. *Crystengcomm* **2016**, *18*, 8396–8405. [CrossRef]
61. Mishra, S.; Debnath, A.; Muthe, K.; Das, N.; Parhi, P. Rapid synthesis of tetragonal zirconia nanoparticles by microwave-solvothermal route and its photocatalytic activity towards organic dyes and hexavalent chromium in single and binary component systems. *Colloids Surf. A-Physicochem. Eng. Asp.* **2021**, *608*, 125551. [CrossRef]
62. Hoffmann, R.; Kaloumenos, M.; Erdem, E.; Weber, S.; Schneider, J. Microwave-Assisted Synthesis, Characterisation and Dielectric Properties of Nanocrystalline Zirconia. *Eur. J. Inorg. Chem.* **2014**, *32*, 5554–5560. [CrossRef]
63. Demazeau, G. Solvothermal Processes: Definition, Key Factors Governing the Involved Chemical Reactions and New Trends. *Z. Naturforsch. B* **2010**, *65*, 999–1006. [CrossRef]
64. Liu, L.; Wang, S.; Jiang, G.; Zhang, B.; Yang, J.; Wang, J.; Liu, W.; Li, Y.; Liu, H. Solvothermal synthesis of zirconia nanomaterials: Latest developments and future. *Ceram. Int.* **2022**, *48*, 32649–32676. [CrossRef]
65. De Keukeleere, K.; De Roo, J.; Lommens, P.; Martins, J.; Van der Voort, P.; Van Driessche, I. Fast and Tunable Synthesis of ZrO_2 Nanocrystals: Mechanistic Insights into Precursor Dependence. *Inorg. Chem.* **2015**, *54*, 3469–3476. [CrossRef] [PubMed]
66. Morris, R. Ionothermal synthesis-ionic liquids as functional solvents in the preparation of crystalline materials. *Chem. Commun.* **2009**, *21*, 2990–2998. [CrossRef] [PubMed]

67. Dong, W.; Lin, F.; Liu, C.; Li, M. Synthesis of ZrO_2 nanowires by ionic-liquid route. *J. Colloid Interface Sci.* **2009**, *333*, 734–740. [CrossRef] [PubMed]
68. Gröhn, A.J.; Pratsinis, S.E.; Sánchez-Ferrer, A.; Mezzenga, R.; Wegner, K. Scale-up of Nanoparticle Synthesis by Flame Spray Pyrolysis: The High-Temperature Particle Residence Time. *Ind. Eng. Chem. Res.* **2014**, *53*, 10734–10742. [CrossRef]
69. Hwangbo, Y.; Lee, Y. Facile synthesis of zirconia nanoparticles using a salt-assisted ultrasonic spray pyrolysis combined with a citrate precursor method. *J. Alloys Compd.* **2019**, *771*, 821–826. [CrossRef]
70. Waghmare, M.; Sonone, P.; Patil, P.; Kadam, V.; Pathan, H.; Ubale, A. Spray Pyrolytic Deposition of Zirconium Oxide Thin Films: Influence of Concentration on Structural and Optical Properties. *Eng. Sci.* **2018**, *5*, 79–87. [CrossRef]
71. Chen, C.; Tseng, T.; Tsai, S.; Lin, C.; Lin, H. Effect of precursor characteristics on zirconia and ceria particle morphology in spray pyrolysis. *Ceram. Int.* **2008**, *34*, 409–416. [CrossRef]
72. Mueller, R.; Jossen, R.; Pratsinis, S.; Watson, M.; Akhtar, M. Zirconia nanoparticles made in spray flames at high production rates. *J. Am. Ceram. Soc.* **2004**, *87*, 197–202. [CrossRef]
73. Rashid, H.U.; Yu, K.; Umar, M.N.; Anjum, M.N.; Khan, K.; Ahmad, N.; Jan, M.T. Catalyst role in chemical vapor deposition (CVD) process: A review. *Rev. Adv. Mater. Sci.* **2015**, *40*, 235–248.
74. Baek, M.; Park, S.; Choi, D. Synthesis of zirconia (ZrO_2) nanowires via chemical vapor deposition. *J. Cryst. Growth* **2017**, *459*, 198–202. [CrossRef]
75. Spear, K.E. Principles and applications of chemical vapor deposition (CVD). *Pure Appl. Chem.* **1982**, *54*, 1297–1311. [CrossRef]
76. Hemmer, E.; Kumakiri, I.; Lecerf, N.; Bredesen, R.; Barth, S.; Altmayer, J.; Donia, N.; Cavelius, C.; Soga, K.; Mathur, S. Nanostructured ZrO_2 membranes prepared by liquid-injection chemical vapor deposition. *Microporous Mesoporous Mater.* **2012**, *163*, 229–236. [CrossRef]
77. Kim, D.Y.; Lee, C.H.; Park, S.J. Preparation of zirconia thin films by metalorganic chemical vapor deposition using ultrasonic nebulization. *J. Mater. Res.* **1996**, *11*, 2583–2587. [CrossRef]
78. Sayago, I.; Hontañón, E.; Aleixandre, M. 9—Preparation of tin oxide nanostructures by chemical vapor deposition. In *Tin Oxide Materials*; Orlandi, M.O., Ed.; Elsevier: Amsterdam, The Netherlands, 2020; pp. 247–280.
79. Pottathara, Y.B.; Grohens, Y.; Kokol, V.; Kalarikkal, N.; Thomas, S. Chapter 1—Synthesis and Processing of Emerging Two-Dimensional Nanomaterials. In *Nanomaterials Synthesis*; Beeran Pottathara, Y., Thomas, S., Kalarikkal, N., Grohens, Y., Kokol, V., Eds.; Elsevier: Amsterdam, The Netherlands, 2019; pp. 1–25.
80. Gedanken, A. Using sonochemistry for the fabrication of nanomaterials. *Ultrason. Sonochem.* **2004**, *11*, 47–55. [CrossRef]
81. Hembram, K.; Rao, G. Microwave Synthesis of Zirconia Nanoparticles. *J. Nanosci. Nanotechnol.* **2008**, *8*, 4159–4162. [CrossRef]
82. Singh, A.; Nakate, U. Microwave Synthesis, Characterization, and Photoluminescence Properties of Nanocrystalline Zirconia. *Sci. World J.* **2014**, *2014*, 349457. [CrossRef]
83. Manjunatha, S.; Dharmaprakash, M. Microwave assisted synthesis of cubic Zirconia nanoparticles and study of optical and photoluminescence properties. *J. Lumin.* **2016**, *180*, 20–24. [CrossRef]
84. Kwon, G.-H.; Kim, T.W.; Lee, H.I.; Cho, W.C.; Kim, H.; Kwon, G.-H.; Kim, T.W.; Lee, H.I.; Cho, W.C.; Kim, H. Synthesis of ZrO_2 nanorods and their application as membrane materials. *J. Korean Ceram. Soc.* **2019**, *56*, 541–548. [CrossRef]
85. Fatimah, I.; Yanti, I.; Suharto, T.E.; Sagadevan, S. ZrO_2-based catalysts for biodiesel production: A review. *Inorg. Chem. Commun.* **2022**, *143*, 109808. [CrossRef]
86. dos Santos, V.; da Silveira, N.; Bergmann, C. In-situ evaluation of particle size distribution of ZrO_2-nanoparticles obtained by sol-gel. *Powder Technol.* **2014**, *267*, 392–397. [CrossRef]
87. Davar, F.; Hassankhani, A.; Loghman-Estarki, M. Controllable synthesis of metastable tetragonal zirconia nanocrystals using citric acid assisted sol-gel method. *Ceram. Int.* **2013**, *39*, 2933–2941. [CrossRef]
88. Madhusudhana, R.; Sangamesha, M.A.; Urs, R.G.K.; Krishnamurthy, L.; Shekar, G.L. synthesis and characterization of zirconia (ZrO_2) by simple sol-gel route. *Int. J. Adv. Res.* **2014**, *2*, 433–436.
89. Ordóñez, F.; Chejne, F.; Pabón, E.; Cacua, K. Synthesis of ZrO_2 nanoparticles and effect of surfactant on dispersion and stability. *Ceram. Int.* **2020**, *46*, 11970–11977. [CrossRef]
90. Dharr, A.; Arjun, A.; Raguram, T.; Rajni, K. Influence of pH on the structural, spectral, optical, morphological and photocatalytic properties of ZrO_2 nanoparticles synthesized by sol-gel technique. *J. Mater. Sci. Mater. Electron.* **2020**, *31*, 15718–15730. [CrossRef]
91. Waghmare, M.; Pawar, K.; Pathan, H.; Ubale, A. Influence of annealing temperature on the structural and optical properties of nanocrystalline zirconium oxide. *Mater. Sci. Semicond. Process.* **2017**, *72*, 122–127. [CrossRef]
92. Huo, H.; Wang, S.; Lin, S.; Li, Y.; Li, B.; Yang, Y. Chiral zirconia nanotubes prepared through a sol–gel transcription approach. *J. Mater. Chem. A* **2014**, *2*, 333–338. [CrossRef]
93. Ijaz, I.; Gilani, E.; Nazir, A.; Bukhari, A. Detail review on chemical, physical and green synthesis, classification, characterizations and applications of nanoparticles. *Green Chem. Lett. Rev.* **2020**, *13*, 59–81. [CrossRef]
94. Wang, N.; Fuh, J.; Dheen, S.; Kumar, A. Synthesis methods of functionalized nanoparticles: A review. *Bio-Des. Manuf.* **2021**, *4*, 379–404. [CrossRef]
95. Parashar, M.; Shukla, V.; Singh, R. Metal oxides nanoparticles via sol-gel method: A review on synthesis, characterization and applications. *J. Mater. Sci.-Mater. Electron.* **2020**, *31*, 3729–3749. [CrossRef]
96. Lopes, N.I.A.; Henrique Jardim Freire, N.; Resende, P.D.; Santos, L.A.; Buono, V.T.L. Electrochemical deposition and characterization of ZrO_2 ceramic nanocoatings on superelastic NiTi alloy. *Appl. Surf. Sci.* **2018**, *450*, 21–30. [CrossRef]

97. Espitia-Cabrera, I.; Orozco-Hernández, H.; Torres-Sánchez, R.; Contreras-García, M.E.; Bartolo-Pérez, P.; Martínez, L. Synthesis of nanostructured zirconia electrodeposited films on AISI 316L stainless steel and its behaviour in corrosion resistance assessment. *Mater. Lett.* **2004**, *58*, 191–195. [CrossRef]
98. Setare, E.; Raeissi, K.; Golozar, M.A.; Fathi, M.H. The structure and corrosion barrier performance of nanocrystalline zirconia electrodeposited coating. *Corros. Sci.* **2009**, *51*, 1802–1808. [CrossRef]
99. Yen, S.-K. Mechanism of electrolytic ZrO_2 coating on commercial pure titanium. *Mater. Chem. Phys.* **2000**, *63*, 256–262. [CrossRef]
100. Liu, B.; Hu, J.; Foord, J.S. Electrochemical Deposition of Zirconia Films on Diamond Electrodes. *Electrochem. Solid-State Lett.* **2011**, *14*, D20. [CrossRef]
101. Giacomelli, F.C.; Giacomelli, C.; De Oliveira, A.G.; Spinelli, A. Effect of electrolytic ZrO_2 coatings on the breakdown potential of NiTi wires used as endovascular implants. *Mater. Lett.* **2005**, *59*, 754–758. [CrossRef]
102. Zhitomirsky, I. Cathodic electrodeposition of ceramic and organoceramic materials. Fundamental aspects. *Adv. Colloid Interface Sci.* **2002**, *97*, 279–317. [CrossRef]
103. Wang, X.; Ghosh, S.K.; Afshar-Mohajer, M.; Zhou, H.; Liu, Y.; Han, X.; Cai, J.; Zou, M.; Meng, X. Atomic layer deposition of zirconium oxide thin films. *J. Mater. Res.* **2020**, *35*, 804–812. [CrossRef]
104. Kukli, K.; Ritala, M.; Leskelä, M. Low-Temperature Deposition of Zirconium Oxide–Based Nanocrystalline Films by Alternate Supply of $Zr[OC(CH_3)_3]_4$ and H_2O. *Chem. Vap. Depos.* **2000**, *6*, 297–302. [CrossRef]
105. Kukli, K.; Kemell, M.; Köykkä, J.; Mizohata, K.; Vehkamäki, M.; Ritala, M.; Leskelä, M. Atomic layer deposition of zirconium dioxide from zirconium tetrachloride and ozone. *Thin Solid Film.* **2015**, *589*, 597–604. [CrossRef]
106. Kukli, K.; Forsgren, K.; Ritala, M.; Leskelä, M.; Aarik, J.; Haårsta, A. Dielectric Properties of Zirconium Oxide Grown by Atomic Layer Deposition from Iodide Precursor. *J. Electrochem. Soc.* **2001**, *148*, F227. [CrossRef]
107. Nam, W.H.; Rhee, S.W. Atomic Layer Deposition of ZrO_2 Thin Films Using Dichlorobis[bis-(trimethylsilyl)amido]zirconium and Water. *Chem. Vap. Depos.* **2004**, *10*, 201–205. [CrossRef]
108. An, J.-K.; Kim, J.-T.; Kang, G.; Oh, N.K.; Hahm, S.-H.; Lee, G.; Park, I.-S.; Yun, J.-Y. ZrO_2 film prepared by atomic layer deposition using less viscous cocktail $CpZr[N(CH_3)_2]_3/C_7H_8$ precursor and ozone. *J. Alloys Compd.* **2017**, *701*, 310–315. [CrossRef]
109. Phung, N.-M.; Ha, M.-T.; Bae, S.-Y.; Lee, S.; Park, T.-J.; Kwon, S.-H.; Jeong, S.-M. Towards modeling of ZrO_2 atomic layer deposition at reactor scale based on experimental kinetic approximation. *Appl. Surf. Sci.* **2024**, *646*, 158840. [CrossRef]
110. Liu, J.; Meng, X.; Banis, M.N.; Cai, M.; Li, R.; Sun, X. Crystallinity-Controlled Synthesis of Zirconium Oxide Thin Films on Nitrogen-Doped Carbon Nanotubes by Atomic Layer Deposition. *J. Phys. Chem. C* **2012**, *116*, 14656–14664. [CrossRef]
111. Liu, J.; Meng, X.; Hu, Y.; Geng, D.; Banis, M.N.; Cai, M.; Li, R.; Sun, X. Controlled synthesis of Zirconium Oxide on graphene nanosheets by atomic layer deposition and its growth mechanism. *Carbon* **2013**, *52*, 74–82. [CrossRef]
112. Vijayaraghavan, K.; Ashokkumar, T. Plant-mediated biosynthesis of metallic nanoparticles: A review of literature, factors affecting synthesis, characterization techniques and applications. *J. Environ. Chem. Eng.* **2017**, *5*, 4866–4883. [CrossRef]
113. Fariq, A.; Khan, T.; Yasmin, A. Microbial synthesis of nanoparticles and their potential applications in biomedicine. *J. Appl. Biomed.* **2017**, *15*, 241–248. [CrossRef]
114. Kumaresan, M.; Anand, K.V.; Govindaraju, K.; Tamilselvan, S.; Kumar, V.G. Seaweed Sargassum wightii mediated preparation of zirconia (ZrO_2) nanoparticles and their antibacterial activity against gram positive and gram negative bacteria. *Microb. Pathog.* **2018**, *124*, 311–315. [CrossRef]
115. Filote, C.; Santos, S.C.; Popa, V.I.; Botelho, C.M.; Volf, I. Biorefinery of marine macroalgae into high-tech bioproducts: A review. *Environ. Chem. Lett.* **2021**, *19*, 969–1000. [CrossRef]
116. Chitoria, A.K.; Mir, A.; Shah, M. A review of ZrO_2 nanoparticles applications and recent advancements. *Ceram. Int.* **2023**, *49*, 32343–32358. [CrossRef]
117. Raj, S.; Hattori, M.; Ozawa, M. Ag-doped ZrO_2 nanoparticles prepared by hydrothermal method for efficient diesel soot oxidation. *Mater. Lett.* **2019**, *234*, 205–207. [CrossRef]
118. Hidayat, D.; Syoufian, A.; Utami, M.; Wijaya, K. Synthesis and application of Na_2O/ZrO_2 nanocomposite for microwave-assisted transesterification of Castor oil. *ICS Phys. Chem.* **2021**, *1*, 26. [CrossRef]
119. Bansal, P.; Kaur, N.; Prakash, C.; Chaudhary, G.R. ZrO_2 nanoparticles: An industrially viable, efficient and recyclable catalyst for synthesis of pharmaceutically significant xanthene derivatives. *Vacuum* **2018**, *157*, 9–16. [CrossRef]
120. Sigwadi, R.; Mokrani, T.; Dhlamini, M. The synthesis, characterization and electrochemical study of zirconia oxide nanoparticles for fuel cell application. *Phys. B Condens. Matter* **2020**, *581*, 411842. [CrossRef]
121. Mir, A.; Shah, M. Cyclic voltammetry response of TiO2 nanostructures prepared via fast and facile microwave irradiation. *Bull. Mater. Sci.* **2022**, *45*, 119. [CrossRef]
122. Mir, A.; Ahmad, R.; Majeed, A.; Sohail, A.; Aalim, M.; Farooq, J.; Shah, M. Microwave-assisted hydrothermal synthesis of Fe-doped TiO_2 photoanode for photocatalytic hydrogen evolution. *ECS J. Solid State Sci. Technol.* **2023**, *12*, 021007. [CrossRef]
123. Goktas, S.; Goktas, A. A comparative study on recent progress in efficient ZnO based nanocomposite and heterojunction photocatalysts: A review. *J. Alloys Compd.* **2021**, *863*, 158734. [CrossRef]
124. Cui, C.; Pu, Y. Improvement of energy storage density with trace amounts of ZrO_2 additives fabricated by wet-chemical method. *J. Alloys Compd.* **2018**, *747*, 495–504. [CrossRef]

125. Gautam, A.; Gautam, C.; Mishra, M.; Sahu, S.; Nanda, R.; Kisan, B.; Gautam, R.K.; Prakash, R.; Sharma, K.; Singh, D. Synthesis, structural, mechanical, and biological properties of HAp-ZrO_2-hBN biocomposites for bone regeneration applications. *Ceram. Int.* **2021**, *47*, 30203–30220. [CrossRef]
126. Whittall, S. Energy conversion and storage. Available online: https://www.theiet.org/publishing/inspec/researching-hot-topics/energy-conversion-and-storage, (accessed on 3 September 2024).
127. Xiang, H.; Liu, Y.; Wang, H.; Song, Y.; Deng, N.; Kang, W. ZrO_2 nanoparticle modified hierarchically porous carbon nanofibers for multifunctional separator with prominent confinement and excellent catalysis of lithium polysulfide for Li-S cell. *J. Energy Storage* **2024**, *92*, 112003. [CrossRef]
128. Ajeena, A.M.; Farkas, I.; Víg, P. Performance enhancement of flat plate solar collector using ZrO_2-SiC/DW hybrid nanofluid: A comprehensive experimental study. *Energy Convers. Manag. X* **2023**, *20*, 100458. [CrossRef]
129. Jaffri, S.B.; Ahmad, K.S.; Abrahams, I.; Kousseff, C.J.; Nielsen, C.B.; Almutairi, B.O. Rare earth (Sm/Eu/Tm) doped ZrO_2 driven electro-catalysis, energy storage, and scaffolding in high-performance perovskite solar cells. *Int. J. Hydrogen Energy* **2023**, *48*, 29119–29141. [CrossRef]
130. Yang, K.; Lee, E.; Lee, D.; Park, J.; Kim, S.; Park, G.; Yu, G.; Lee, J.; Kim, G.; Park, M. Energy conversion and storage using artificially induced antiferroelectricity in HfO_2/ZrO_2 nanolaminates. *Compos. Part B-Eng.* **2022**, *236*, 109824. [CrossRef]
131. Besisa, D.H.; Ewais, E.M.; Ahmed, Y.M. A comparative study of thermal conductivity and thermal emissivity of high temperature solar absorber of ZrO_2/Fe_2O_3 and Al_2O_3/CuO ceramics. *Ceram. Int.* **2021**, *47*, 28252–28259. [CrossRef]
132. Idrissi, S.; Ziti, S.; Labrim, H.; Bahmad, L. Sulfur doping effect on the electronic properties of zirconium dioxide ZrO_2. *Mater. Sci. Eng. B* **2021**, *270*, 115200. [CrossRef]
133. Sakthisharmila, P.; Sivakumar, N.; Mathupriya, J. Synthesis, characterization of Mn, Fe doped ZrO_2 composites and its applications on photocatalytic and solar catalytic studies. *Mater. Today Proc.* **2021**, *47*, 2159–2167. [CrossRef]
134. Lee, H.; Kim, K.; Song, O. Properties of Double Electron Transport Layered Perovskite Solar Cells with Different ZrO_2 Layer Thickness. *Korean J. Met. Mater.* **2020**, *58*, 59–66. [CrossRef]
135. Doroshkevich, A.; Asgerov, E.; Shylo, A.; Lyubchyk, A.; Logunov, A.; Glazunova, V.; Islamov, A.; Turchenko, V.; Almasan, V.; Lazar, D.; et al. Direct conversion of the water adsorption energy to electricity on the surface of zirconia nanoparticles. *Appl. Nanosci.* **2019**, *9*, 1603–1609. [CrossRef]
136. Bhosale, R. Synthesis and characterization of nanocrystalline $CoFe_2O_4$-zirconia via propylene oxide aided sol-gel method. *Ceram. Int.* **2018**, *44*, 8679–8683. [CrossRef]
137. Doroshkevich, A.; Lyubchyk, A.; Shilo, A.; Zelenyak, T.; Glazunova, V.; Burhovetskiy, V.; Saprykina, A.; Holmurodov, K.; Nosolev, I.; Doroshkevich, V.; et al. Chemical-Electric Energy Conversion Effect in Zirconia Nanopowder Systems. *J. Surf. Investig.* **2017**, *11*, 523–529. [CrossRef]
138. Jin, E.; Park, J.; Zhao, X.; Lee, I.; Jeong, S.; Gu, H. Photovoltaic properties of TiO_2-ZrO_2 fiber composite electrodes for dye-sensitized solar cells. *Mater. Lett.* **2014**, *126*, 281–284. [CrossRef]
139. Barea, E.; Xu, X.; González-Pedro, V.; Ripollés-Sanchis, T.; Fabregat-Santiago, F.; Bisquert, J. Origin of efficiency enhancement in Nb_2O_5 coated titanium dioxide nanorod based dye sensitized solar cells. *Energy Environ. Sci.* **2011**, *4*, 3414–3419. [CrossRef]
140. Tachan, Z.; Hod, I.; Shalom, M.; Grinis, L.; Zaban, A. The importance of the TiO_2/quantum dots interface in the recombination processes of quantum dot sensitized solar cells. *Phys. Chem. Chem. Phys.* **2013**, *15*, 3841–3845. [CrossRef] [PubMed]
141. Liu, Z.; Miyauchi, M.; Uemura, Y.; Cui, Y.; Hara, K.; Zhao, Z.; Sunahara, K.; Furube, A. Enhancing the performance of quantum dots sensitized solar cell by SiO_2 surface coating. *Appl. Phys. Lett.* **2010**, *96*, 233107. [CrossRef]
142. Diaz-Torres, L.; Salas, P.; Angeles-Chavez, C.; Meza, O.; Lopez-Luke, T. Green upconversion emission dependence on size and surface residual contaminants in nanocrystalline ZrO_2: Er^{3+}. *J. Sol-Gel Sci. Technol.* **2012**, *63*, 473–480. [CrossRef]
143. Diaz-Torres, L.; Meza, O.; Solis, D.; Salas, P.; De la Rosa, E. Visible upconversion emission and non-radiative direct Yb^{3+} to Er^{3+} energy transfer processes in nanocrystalline ZrO_2: Yb^{3+}, Er^{3+}. *Opt. Lasers Eng.* **2011**, *49*, 703–708. [CrossRef]
144. Zhang, H.; Fu, X.; Niu, S.; Xin, Q. Blue emission of ZrO_2: Tm nanocrystals with different crystal structure under UV excitation. *J. Non-Cryst. Solids* **2008**, *354*, 1559–1563. [CrossRef]
145. Dong, C.; Li, X.; Qi, J. First-principles investigation on electronic properties of quantum dot-sensitized solar cells based on anatase TiO_2 nanotubes. *J. Phys. Chem. C* **2011**, *115*, 20307–20315. [CrossRef]
146. Krebs, F.C.; Gevorgyan, S.A.; Alstrup, J. A roll-to-roll process to flexible polymer solar cells: Model studies, manufacture and operational stability studies. *J. Mater. Chem.* **2009**, *19*, 5442–5451. [CrossRef]
147. Helgesen, M.; Søndergaard, R.; Krebs, F.C. Advanced materials and processes for polymer solar cell devices. *J. Mater. Chem.* **2010**, *20*, 36–60. [CrossRef]
148. Cerdán-Pasarán, A.; Lopez-Luke, T.; Esparza, D.; Zarazúa, I.; De la Rosa, E.; Fuentes-Ramírez, R.; Alatorre-Ordaz, A.; Sánchez-Solís, A.; Torres-Castro, A.; Zhang, J.Z. Photovoltaic properties of multilayered quantum dot/quantum rod-sensitized TiO_2 solar cells fabricated by SILAR and electrophoresis. *Phys. Chem. Chem. Phys.* **2015**, *17*, 18590–18599. [CrossRef] [PubMed]
149. Esparza, D.; Zarazúa, I.; López-Luke, T.; Cerdán-Pasarán, A.; Sánchez-Solís, A.; Torres-Castro, A.; Mora-Sero, I.; De la Rosa, E. Effect of different sensitization technique on the photoconversion efficiency of CdS quantum dot and CdSe quantum rod sensitized TiO2 solar cells. *J. Phys. Chem. C* **2015**, *119*, 13394–13403. [CrossRef]
150. Zhu, H.; Li, J.; Chen, K.; Yi, X.; Cheng, S.; Gan, F. Nature of charge transport and p-electron ferromagnetism in nitrogen-doped ZrO_2: An ab initio perspective. *Sci. Rep.* **2015**, *5*, 8586. [CrossRef] [PubMed]

151. Yang, F.; Bao, Y.; Zeng, B.; Wu, J.; Li, X.; Sun, Y.; Chen, Y.; Wang, G. Excellent energy storage properties in ZrO_2 toughened $Ba_{0.55}Sr_{0.45}TiO_3$-based relaxor ferroelectric ceramics via multi-scale synergic regulation. *Chem. Eng. J.* **2024**, *493*, 152624. [CrossRef]
152. Akune, T.; Morita, Y.; Shirakawa, S.; Katagiri, K.; Inumaru, K. ZrO_2 nanocrystals as catalyst for synthesis of dimethylcarbonate from methanol and carbon dioxide: Catalytic activity and elucidation of active sites. *Langmuir* **2018**, *34*, 23–29. [CrossRef]
153. Kauppi, E.; Honkala, K.; Krause, A.; Kanervo, J.; Lefferts, L. ZrO_2 acting as a redox catalyst. *Top. Catal.* **2016**, *59*, 823–832. [CrossRef]
154. Neris, A.M.; Ferreira, J.M.; Fonseca, M.G.; dos Santos, I.M.G. Undoped tetragonal ZrO_2 obtained by the Pechini method: Thermal evaluation of tetragonal–monoclinic phase transition and application as catalyst for biodiesel synthesis. *J. Therm. Anal. Calorim.* **2021**, *143*, 3307–3316. [CrossRef]
155. Aguila, G.; Salinas, D.; Jiménez, R.; Guerrero, S.; Araya, P. ZrO_2-supported alkali metal (Li, Na, K) catalysts for biodiesel production. *J. Chil. Chem. Soc.* **2016**, *61*, 3233–3238. [CrossRef]
156. Sharma, Y.C.; Singh, B.; Korstad, J. Advancements in solid acid catalysts for ecofriendly and economically viable synthesis of biodiesel. *Biofuels Bioprod. Biorefin.* **2011**, *5*, 69–92. [CrossRef]
157. Mazzei, A.; Rodrigues, J. Alumina-mullite-zirconia composites obtained by reaction sintering: Part I. Microstructure and mechanical behaviour. *J. Mater. Sci.* **2000**, *35*, 2807–2814. [CrossRef]
158. Theunissen, G.; Bouma, J.; Winnubst, A.; Burggraaf, A. Mechanical properties of ultra-fine grained zirconia ceramics. *J. Mater. Sci.* **1992**, *27*, 4429–4438. [CrossRef]
159. Besisa, D.H.; Ewais, E.M. Black zirconia composites with enhanced thermal, optical and mechanical performance for solar energy applications. *Sol. Energy Mater. Sol. Cells* **2021**, *225*, 111063. [CrossRef]
160. Fend, T. High porosity materials as volumetric receivers for solar energetics. *Opt. Appl.* **2010**, *40*, 271–284.
161. Besisa, D.H.; Ewais, E.M.; Shalaby, E.A.; Usenko, A.; Kuznetsov, D.V. Thermoelectric properties and thermal stress simulation of pressureless sintered SiC/AlN ceramic composites at high temperatures. *Sol. Energy Mater. Sol. Cells* **2018**, *182*, 302–313. [CrossRef]
162. Besisa, D.H.; Ewais, E.M.; Ahmed, Y.M.; Elhosiny, F.I.; Fend, T.; Kuznetsov, D.V. Thermal shock resistance of pressureless sintered SiC/AlN ceramic composites. *Mater. Res. Express* **2018**, *5*, 015506. [CrossRef]
163. Besisa, D.H.; Ewais, E.M.; Ahmed, Y.M.; Elhosiny, F.I.; Fend, T.; Kuznetsov, D.V. Investigation of microstructure and mechanical strength of SiC/AlN composites processed under different sintering atmospheres. *J. Alloys Compd.* **2018**, *756*, 175–181. [CrossRef]
164. Sani, E.; Mercatelli, L.; Fontani, D.; Sans, J.-L.; Sciti, D. Hafnium and tantalum carbides for high temperature solar receivers. *J. Renew. Sustain. Energy* **2011**, *3*, 063107. [CrossRef]
165. Fend, T.; Hoffschmidt, B.; Pitz-Paal, R.; Reutter, O.; Rietbrock, P. Porous materials as open volumetric solar receivers: Experimental determination of thermophysical and heat transfer properties. *Energy* **2004**, *29*, 823–833. [CrossRef]
166. Fang, J.; Tu, N.; Wei, J. Effects of absorber emissivity on thermal performance of a solar cavity receiver. *Adv. Condens. Matter Phys.* **2014**, *2014*, 564639. [CrossRef]
167. Besisa, D.H.; Ewais, E.M.; Mohamed, E.A.; Besisa, N.H.; Ahmed, Y.M. Inspection of thermal stress parameters of high temperature ceramics and energy absorber materials. *Sol. Energy Mater. Sol. Cells* **2019**, *203*, 110160. [CrossRef]
168. Kennedy, C.E. *Review of Mid- to High-Temperature Solar Selective Absorber Materials*; National Renewable Energy Lab (NREL): Golden, CO, USA, 2002.
169. Rashmi, M.; Sagar, P.S.; Devi, N.L.; Sreedhar, V.; Devi, N.G.; Sakhare, D. Analyzing performance of a solar water heater using nano-ZrO_2/water-based nanofluid. *Mater. Today Proc.* 2023; *in press*. [CrossRef]
170. Faizal, M.; Saidur, R.; Mekhilef, S.; Alim, M. Energy, economic and environmental analysis of metal oxides nanofluid for flat-plate solar collector. *Energy Convers. Manag.* **2013**, *76*, 162–168. [CrossRef]
171. Wahab, A.; Hassan, A.; Qasim, M.A.; Ali, H.M.; Babar, H.; Sajid, M.U. Solar energy systems–potential of nanofluids. *J. Mol. Liq.* **2019**, *289*, 111049. [CrossRef]
172. Sheikholeslami, M.; Farshad, S.A.; Ebrahimpour, Z.; Said, Z. Recent progress on flat plate solar collectors and photovoltaic systems in the presence of nanofluid: A review. *J. Clean. Prod.* **2021**, *293*, 126119. [CrossRef]
173. Srinivasan, S.; Vivek, C.; Sakthivel, P.; Chamundeeswari, G.; Bharathi, S.P.; Amuthameena, S.; Balraj, B. Synthesis of Ag incorporated ZrO_2 nanomaterials for enhanced electrochemical energy storage applications. *Inorg. Chem. Commun.* **2022**, *138*, 109262. [CrossRef]
174. Abdel Maksoud, M.; Fahim, R.A.; Shalan, A.E.; Abd Elkodous, M.; Olojede, S.; Osman, A.I.; Farrell, C.; Al-Muhtaseb, A.A.H.; Awed, A.; Ashour, A. Advanced materials and technologies for supercapacitors used in energy conversion and storage: A review. *Environ. Chem. Lett.* **2021**, *19*, 375–439. [CrossRef]
175. Sarı, A.; Saleh, T.A.; Hekimoğlu, G.; Tyagi, V.; Sharma, R. Microencapsulated heptadecane with calcium carbonate as thermal conductivity-enhanced phase change material for thermal energy storage. *J. Mol. Liq.* **2021**, *328*, 115508. [CrossRef]
176. Majumdar, D.; Mandal, M.; Bhattacharya, S.K. Journey from supercapacitors to supercapatteries: Recent advancements in electrochemical energy storage systems. *Emergent Mater.* **2020**, *3*, 347–367. [CrossRef]
177. Owusu, P.A.; Asumadu-Sarkodie, S. A review of renewable energy sources, sustainability issues and climate change mitigation. *Cogent Eng.* **2016**, *3*, 1167990. [CrossRef]
178. Gielen, D.; Boshell, F.; Saygin, D.; Bazilian, M.D.; Wagner, N.; Gorini, R. The role of renewable energy in the global energy transformation. *Energy Strategy Rev.* **2019**, *24*, 38–50. [CrossRef]

179. Sung, J.; Shin, C. Recent studies on supercapacitors with next-generation structures. *Micromachines* **2020**, *11*, 1125. [CrossRef] [PubMed]
180. Mirzaeian, M.; Abbas, Q.; Hunt, M.R.; Hall, P. Pseudocapacitive effect of carbons doped with different functional groups as electrode materials for electrochemical capacitors. *Energies* **2020**, *13*, 5577. [CrossRef]
181. Abdah, M.A.A.M.; Azman, N.H.N.; Kulandaivalu, S.; Sulaiman, Y. Review of the use of transition-metal-oxide and conducting polymer-based fibres for high-performance supercapacitors. *Mater. Des.* **2020**, *186*, 108199. [CrossRef]
182. Mudila, H.; Rana, S.; Zaidi, M. Electrochemical performance of zirconia/graphene oxide nanocomposites cathode designed for high power density supercapacitor. *J. Anal. Sci. Technol.* **2016**, *7*, 3. [CrossRef]
183. Wang, X.; Chen, J.; Zheng, M.; Yang, F.; Shao, D.; Hao, Y.; Liang, T.; Feng, J.; Liu, C.; Yu, K. Improvement of the energy storage performance in Pb0. 88La0. 12ZrO3 thin films by inserting ZrO_2 layer. *Phys. B Condens. Matter* **2023**, *665*, 415073. [CrossRef]
184. Shrivastav, V.; Sundriyal, S.; Tiwari, U.; Kim, K.; Deep, A. Metal-organic framework derived zirconium oxide/carbon composite as an improved supercapacitor electrode. *Energy* **2021**, *235*, 121351. [CrossRef]
185. Kaur, M.; Pal, K. Potential electrochemical hydrogen storage in nickel and cobalt nanoparticles-induced zirconia-graphene nanocomposite. *J. Mater. Sci. Mater. Electron.* **2020**, *31*, 10903–10911. [CrossRef]
186. Wang, J.; Sun, Y.; Wang, P.; Yu, X.; Shi, H.; Zhang, X.; Yang, H.; Lin, B. High energy density of polyimide composites containing one-dimensional $BaTiO_3$@ZrO_2 nanofibers for energy storage device. *J. Alloys Compd.* **2019**, *789*, 785–791. [CrossRef]
187. Do Kim, K.; Lee, Y.; Gwon, T.; Kim, Y.; Kim, H.; Moon, T.; Hyun, S.; Park, H.; Park, M.; Hwang, C. Scale-up and optimization of HfO_2-ZrO_2 solid solution thin films for the electrostatic supercapacitors. *Nano Energy* **2017**, *39*, 390–399. [CrossRef]
188. Kaur, M.; Pal, K. An investigation for hydrogen storage capability of zirconia-reduced graphene oxide nanocomposite. *Int. J. Hydrogen Energy* **2016**, *41*, 21861–21869. [CrossRef]
189. Guo, D.; Lu, Y.; Zhao, Y.; Zhang, X. Synthesis and physicochemical properties of graphene/ZrO_2 composite aerogels. *RSC Adv.* **2015**, *5*, 11738–11744. [CrossRef]
190. Pan, W.; Liu, B.; Li, Z. Hydrogen storage performance of 2LiH+MgB_2 doped with hydrothermal-synthesized ZrO_2 nanorods. *Int. J. Hydrogen Energy* **2014**, *39*, 15595–15603. [CrossRef]
191. Rajangam, K.; Amuthameena, S.; Thangavel, S.; Sanjanadevi, V.S.; Balraj, B. Synthesis and characterisation of Ag incorporated TiO_2 nanomaterials for supercapacitor applications. *J. Mol. Struct.* **2020**, *1219*, 128661. [CrossRef]
192. Kim, S.; Kim, Y.J.; Ryu, W.-H. Zirconium disulfides as an electrode material alternative for Li-ion batteries. *Appl. Surf. Sci.* **2021**, *547*, 149029. [CrossRef]
193. Manzoor, S.; Ashiq, M.F.; Usman, M.; Sadaqat, M.; Mahmood, K.; Munawar, T.; Iqbal, F.; Al-Anazy, M.M.; Ashiq, M.N.; Najam-ul-Haq, M. Development of excellent and novel flowery zirconia/cadmium sulfide nanohybrid electrode: For high performance electrochemical supercapacitor application. *J. Energy Storage* **2021**, *40*, 102718. [CrossRef]
194. Jinxi, W.; Aimin, W.; Ghasemi, A.K.; Lashkenari, M.S.; Pashai, E.; Karaman, C.; Niculina, D.E.; Karimi-Maleh, H. Tailoring of $ZnFe_2O_4$-ZrO_2-based nanoarchitectures catalyst for supercapacitor electrode material and methanol oxidation reaction. *Fuel* **2023**, *334*, 126685. [CrossRef]
195. Arifin, D.; Ambrosini, A.; Wilson, S.A.; Mandal, B.; Muhich, C.L.; Weimer, A.W. Investigation of Zr, Gd/Zr, and Pr/Zr—Doped ceria for the redox splitting of water. *Int. J. Hydrogen Energy* **2020**, *45*, 160–174. [CrossRef]
196. Mir, W.J.; Sheikh, T.; Arfin, H.; Xia, Z.; Nag, A. Lanthanide doping in metal halide perovskite nanocrystals: Spectral shifting, quantum cutting and optoelectronic applications. *NPG Asia Mater.* **2020**, *12*, 9. [CrossRef]
197. Nasibi, M.; Golozar, M.A.; Rashed, G. Nano zirconium oxide/carbon black as a new electrode material for electrochemical double layer capacitors. *J. Power Sources* **2012**, *206*, 108–110. [CrossRef]
198. Yasin, A.S.; Mohamed, I.M.A.; Park, C.H.; Kim, C.S. Design of novel electrode for capacitive deionization using electrospun composite titania/zirconia nanofibers doped-activated carbon. *Mater. Lett.* **2018**, *213*, 62–66. [CrossRef]
199. Selvi, N.; Sankar, S.; Dinakaran, K. Synthesis, structural and optical characterization of ZrO_2 core–ZnO@SiO_2 shell nanoparticles prepared using co-precipitation method for opto-electronic applications. *J. Mater. Sci. Mater. Electron.* **2014**, *25*, 5078–5083. [CrossRef]
200. Abhisek, K.; Vhatkar, S.; Mathew, H.; Srivastava, D.; Oraon, R. Unravelling the Growth Mechanism of Nanotorous ZrO_2-NiO Binary Composite and its Electrochemical Study for Supercapacitor Application. *J. Clust. Sci.* **2024**, *35*, 3045–3063. [CrossRef]
201. Mohsen, Q.; Al-Gethami, W.S.; Zaki, Z.; Alotaibi, S.H.; Ibrahim, M.M.; Ezzat, M.; Amin, M.A.; Kamel, M.M.; Mostafa, N.Y. Effect of pH on Hydrothermal Synthesis of ZrO_2 Nanoparticles and their Electrocatalytic Activity for Hydrogen Production. *Int. J. Electrochem. Sci.* **2022**, *17*, 22073. [CrossRef]
202. Pérez-Tomás, A.; Lira-Cantú, M.; Catalan, G. Above-Bandgap Photovoltages in Antiferroelectrics. *Adv. Mater.* **2016**, *28*, 9644–9647. [CrossRef]
203. Starkiewicz, J.; Sosnowski, L.; Simpson, O. Photovoltaic Effects Exhibited in High-resistance Semi-conducting Films. *Nature* **1946**, *158*, 28. [CrossRef]
204. Hao, X.; Zhai, J.; Yang, J.; Ren, H.; Song, X. Improved field-induced strains and fatigue endurance of PLZT antiferroelectric thick films by orientation control. *Phys. Status Solidi RRL—Rapid Res. Lett.* **2009**, *3*, 248–250. [CrossRef]
205. Hao, X.; Zhai, J.; Kong, L.B.; Xu, Z. A comprehensive review on the progress of lead zirconate-based antiferroelectric materials. *Prog. Mater. Sci.* **2014**, *63*, 1–57. [CrossRef]

206. Lan, D.; Gao, R.; Liu, X.; Zhu, L.; Zheng, Y.; Liu, J. Microstructure and mechanical properties of ZrO_2 fiber toughened $Al_2O_3/ZrO_2(Y_2O_3)$ solidified ceramics prepared with high frequency induction zone melting. *J. Alloys Compd.* **2023**, *967*, 171669. [CrossRef]
207. Lee, J.H.; Yoshikawa, A.; Kaiden, H.; Lebbou, K.; Fukuda, T.; Yoon, D.H.; Waku, Y. Microstructure of Y_2O_3 doped Al_2O_3/ZrO_2 eutectic fibers grown by the micro-pulling-down method. *J. Cryst. Growth* **2001**, *231*, 179–185. [CrossRef]
208. Dharshini, A.; Adhikari, S.; Rajendran, N. Surface engineering of zirconium with chitosan PEDOT for enhanced bioactivity and corrosion behavior. *J. Alloys Compd.* **2024**, *977*, 173384. [CrossRef]
209. Abbasi, E.; Milani, M.; Fekri Aval, S.; Kouhi, M.; Akbarzadeh, A.; Tayefi Nasrabadi, H.; Nikasa, P.; Joo, S.W.; Hanifehpour, Y.; Nejati-Koshki, K. Silver nanoparticles: Synthesis methods, bio-applications and properties. *Crit. Rev. Microbiol.* **2016**, *42*, 173–180. [CrossRef] [PubMed]
210. Al-nayili, A.; Idan, A. Environmentally friendly production, characterization, and utilization of ZrO_2 nanoparticles for the adsorption of amoxicillin in water solutions. *J. Mol. Liq.* **2023**, *389*, 122875. [CrossRef]
211. Da'na, E.; Hassanin, H.; Taha, A.; El-Aassar, M. Microwave-Aided Green Synthesis of $ZrO_2/ZnO/AC$ Nanocomposite for Catalytic Degradation of Organic Dye. *Water Air Soil Pollut.* **2023**, *234*, 436. [CrossRef]
212. Alagarsamy, A.; Chandrasekaran, S.; Manikandan, A. Green synthesis and characterization studies of biogenic zirconium oxide (ZrO_2) nanoparticles for adsorptive removal of methylene blue dye. *J. Mol. Struct.* **2022**, *1247*, 131275. [CrossRef]
213. Al-Zaqri, N.; Muthuvel, A.; Jothibas, M.; Alsalme, A.; Alharthi, F.; Mohana, V. Biosynthesis of zirconium oxide nanoparticles using Wrightia tinctoria leaf extract: Characterization, photocatalytic degradation and antibacterial activities. *Inorg. Chem. Commun.* **2021**, *127*, 108507. [CrossRef]
214. Debnath, B.; Majumdar, M.; Bhowmik, M.; Bhowmik, K.L.; Debnath, A.; Roy, D.N. The effective adsorption of tetracycline onto zirconia nanoparticles synthesized by novel microbial green technology. *J. Environ. Manag.* **2020**, *261*, 110235. [CrossRef]
215. Rasheed, P.; Haq, S.; Waseem, M.; Rehman, S.; Rehman, W.; Bibi, N.; Shah, S. Green synthesis of vanadium oxide-zirconium oxide nanocomposite for the degradation of methyl orange and picloram. *Mater. Res. Express* **2020**, *7*, 025011. [CrossRef]
216. da Silva, A.F.V.; Fagundes, A.P.; Macuvele, D.L.P.; de Carvalho, E.F.U.; Durazzo, M.; Padoin, N.; Soares, C.; Riella, H.G. Green synthesis of zirconia nanoparticles based on *Euclea natalensis* plant extract: Optimization of reaction conditions and evaluation of adsorptive properties. *Colloids Surf. A Physicochem. Eng. Asp.* **2019**, *583*, 123915. [CrossRef]
217. Shinde, H.; Bhosale, T.; Gavade, N.; Babar, S.; Kamble, R.; Shirke, B.; Garadkar, K. Biosynthesis of ZrO_2 nanoparticles from *Ficus benghalensis* leaf extract for photocatalytic activity. *J. Mater. Sci. Mater. Electron.* **2018**, *29*, 14055–14064. [CrossRef]
218. Saraswathi, V.; Santhakumar, K. Photocatalytic activity against azo dye and cytotoxicity on MCF-7 cell lines of zirconium oxide nanoparticle mediated using leaves of *Lagerstroemia speciosa*. *J. Photochem. Photobiol. B-Biol.* **2017**, *169*, 47–55. [CrossRef]
219. Gurushantha, K.; Anantharaju, K.; Sharma, S.; Nagaswarupa, H.; Prashantha, S.; Mahesh, K.; Renuka, L.; Vidya, Y.; Nagabhushana, H. Bio-mediated Sm doped nano cubic zirconia: Photoluminescent, Judd-Ofelt analysis, electrochemical impedance spectroscopy and photocatalytic performance. *J. Alloys Compd.* **2016**, *685*, 761–773. [CrossRef]
220. Renuka, L.; Anantharaju, K.; Sharma, S.; Nagaswarupa, H.; Prashantha, S.; Nagabhushana, H.; Vidya, Y. Hollow microspheres Mg-doped ZrO_2 nanoparticles: Green assisted synthesis and applications in photocatalysis and photoluminescence. *J. Alloys Compd.* **2016**, *672*, 609–622. [CrossRef]
221. Prasad, K.S.; Amin, Y.; Selvaraj, K. Defluoridation using biomimetically synthesized nano zirconium chitosan composite: Kinetic and equilibrium studies. *J. Hazard. Mater.* **2014**, *276*, 232–240. [CrossRef]
222. Van Tran, T.; Nguyen, D.T.C.; Le, H.T.N.; Ho, H.L.; Nguyen, T.T.; Doan, V.-D.; Nguyen, T.D.; Bach, L.G. Response surface methodology-optimized removal of chloramphenicol pharmaceutical from wastewater using $Cu_3(BTC)_2$-derived porous carbon as an efficient adsorbent. *Comptes Rendus. Chim.* **2019**, *22*, 794–803. [CrossRef]
223. Van Tran, T.; Nguyen, D.T.C.; Nguyen, T.T.; Le, H.T.; Van Nguyen, C.; Nguyen, T.D. Metal-organic framework HKUST-1-based $Cu/Cu_2O/CuO@C$ porous composite: Rapid synthesis and uptake application in antibiotics remediation. *J. Water Process Eng.* **2020**, *36*, 101319. [CrossRef]
224. Dang, H.H.; Nguyen, D.T.C.; Nguyen, T.T.; Nguyen, T.T.T.; Vo, D.-V.N.; Nguyen, T.D.; Lee, T.; Van Tran, T. Zeolitic-imidazolate framework-derived N-self-doped porous carbons with ultrahigh theoretical adsorption capacities for tetracycline and ciprofloxacin. *J. Environ. Chem. Eng.* **2021**, *9*, 104938. [CrossRef]
225. Nguyen, D.T.C.; Dang, H.H.; Vo, D.-V.N.; Bach, L.G.; Nguyen, T.D.; Tran, T.V. Biogenic synthesis of MgO nanoparticles from different extracts (flower, bark, leaf) of *Tecoma stans* (L.) and their utilization in selected organic dyes treatment. *J. Hazard. Mater.* **2021**, *404*, 124146. [CrossRef]
226. Nguyen, D.T.C.; Le, H.T.N.; Nguyen, T.T.; Nguyen, T.T.T.; Bach, L.G.; Nguyen, T.D.; Tran, T.V. Multifunctional ZnO nanoparticles bio-fabricated from *Canna indica* L. flowers for seed germination, adsorption, and photocatalytic degradation of organic dyes. *J. Hazard. Mater.* **2021**, *420*, 126586. [CrossRef]
227. Padovini, D.S.S.; Magdalena, A.G.; Capeli, R.G.; Longo, E.; Dalmaschio, C.J.; Chiquito, A.J.; Pontes, F.M. Synthesis and characterization of $ZrO_2@SiO_2$ core-shell nanostructure as nanocatalyst: Application for environmental remediation of rhodamine B dye aqueous solution. *Mater. Chem. Phys.* **2019**, *233*, 1–8. [CrossRef]
228. Affonso, L.N.; Marques, J.L., Jr.; Lima, V.V.; Gonçalves, J.O.; Barbosa, S.C.; Primel, E.G.; Burgo, T.A.; Dotto, G.L.; Pinto, L.A.; Cadaval, T.R., Jr. Removal of fluoride from fertilizer industry effluent using carbon nanotubes stabilized in chitosan sponge. *J. Hazard. Mater.* **2020**, *388*, 122042. [CrossRef]

229. Majedi, A.; Abbasi, A.; Davar, F. Green synthesis of zirconia nanoparticles using the modified Pechini method and characterization of its optical and electrical properties. *J. Sol-Gel Sci. Technol.* **2016**, *77*, 542–552. [CrossRef]
230. Vennila, R.; Kamaraj, P.; Arthanareeswari, M.; Sridharan, M.; Sudha, G.; Devikala, S.; Arockiaselvi, J.; Sivakumar, B.; Rajeshwari, K. Biosynthesis of ZrO nanoparticles and its natural dye sensitized solar cell studies. *Mater. Today Proc.* **2018**, *5*, 8691–8698. [CrossRef]
231. Devikala, S.; Kamaraj, P.; Arthanareeswari, M. Corrosion resistance behavior of PVDF/ZrO_2 composite in 3.5% NaCl. *Mater. Today Proc.* **2019**, *14*, 279–287. [CrossRef]
232. Kumar, N.; Irfan, G. A review on tribological behaviour and mechanical properties of Al/ZrO_2 metal matrix nano composites. *Mater. Today Proc.* **2021**, *38*, 2649–2657. [CrossRef]
233. Huang, W.; Qiu, H.; Zhang, Y.; Nan, L.; Gao, L.; Chen, J.; Omran, M.; Chen, G. Preparation of nano zirconia by binary doping: Effect of controlled sintering on structure and phase transformation. *Ceram. Int.* **2022**, *48*, 25374–25381. [CrossRef]
234. Vattikuti, S.P.; Prasad, P.R.; Aljuwayid, A.M.; Rosaiah, P.; Sudhani, H.P.; Shim, J. Enhanced solar light-induced performance of a step-scheme heterojunction nanostructure (C_3N_4/ZrO_2) for mixed dye degradation and methanol oxidation. *Mater. Sci. Semicond. Process.* **2024**, *177*, 108342. [CrossRef]